A mosaic of phytoplankton responses across Patagonia, the southeast Pacific and southwest Atlantic Oceans to ash deposition and trace metal release from the Calbuco volcanic eruption in 2015

Maximiliano J. Vergara-Jara[1,2], Mark J. Hopwood[3*], Thomas J. Browning[3], Insa Rapp[4], Rodrigo Torres[2,5], Brian Reid[5], Eric P. Achterberg[3], José Luis Iriarte[2,6].

[1]Programa de Doctorado en Ciencias de la Acuicultura, Universidad Austral de Chile, Puerto Montt, Chile.

[2]Instituto de Acuicultura & Centro de Investigación Dinámica de Ecosistemas Marinos de Altas Latitudes - IDEAL, Universidad Austral de Chile, Puerto Montt, Chile.

[3]GEOMAR, Helmholtz Centre for Ocean Research, 24148 Kiel, Germany.

[4]Department of Biology, Dalhousie University, Halifax, Nova Scotia, Canada

[5]Centro de Investigación en Ecosistemas de la Patagonia (CIEP), Coyhaique, Chile.

[6]COPAS-Sur Austral, Centro de Investigación Oceanográfica en el Pacífico Sur-Oriental (COPAS), Universidad de Concepción, Concepción, Chile.

Key words: volcanic ash, iron, Fe(II), phytoplankton, carbonate chemistry, Reloncaví Fjord

Corresponding author*: mhopwood@geomar.de

Abstract

Following the eruption of the Calbuco volcano in April 2015, an extensive ash plume spread across northern Patagonia and into the southeast Pacific and southwest Atlantic Oceans. Here we report on field surveys conducted in the coastal region receiving the highest ash load following the eruption (Reloncaví Fjord). The fortuitous location of a long-term monitoring station in Reloncaví Fjord provided data to evaluate inshore phytoplankton bloom dynamics and carbonate chemistry during April-May 2015. Satellite derived chlorophyll-a measurements over the ocean regions affected by the ash plume in May 2015 were obtained to determine the spatial-temporal gradients in offshore phytoplankton response to ash. Additionally, leaching experiments were performed to quantify the release from ash into solution of total alkalinity, trace elements (dissolved Fe, Mn, Pb, Co, Cu, Ni and Cd) and major ions (F^-, Cl^-, SO_4^{2-}, NO_3^-, Li^+, Na^+, NH_4^+, K^+, Mg^{2+}, Ca^{2+}). Within Reloncaví Fjord, integrated peak diatom abundances during the May 2015 austral bloom were approximately 2-4 times higher than usual (up to 1.4×10^{11} cells m^{-2}, integrated to 15 m depth), with the bloom intensity perhaps moderated due to high ash loadings in the two weeks following the eruption. Any mechanistic link between ash deposition and the Reloncaví diatom bloom can however only be speculated on due to the lack of data immediately preceding and following the eruption. In the offshore southeast Pacific, a short duration phytoplankton bloom corresponded closely in space and time to the maximum observed ash plume, potentially in response to Fe-fertilization of a region where phytoplankton growth is typically Fe-limited at this time of year. Conversely, no clear fertilization on the same time-scale was found in the area subject to an ash plume over the southwest Atlantic where the availability of fixed nitrogen is thought to limit phytoplankton growth. This was consistent with no significant release of fixed nitrogen (NO_x or NH_4) from Calbuco ash.

In addition to release of nanomolar concentrations of dissolved Fe from ash suspended in seawater, it was observed that low loadings (< 5 mg L^{-1}) of ash were an unusually prolific source of Fe(II) into chilled seawater (up to 1.0 µmol Fe g^{-1}), producing a pulse of Fe(II) typically released mainly during the first minute after addition to seawater. This release would not be detected, either as Fe(II) or dissolved Fe, following standard leaching protocols at room temperature. A pulse of Fe(II) release upon addition of Calbuco ash to seawater made it an unusually efficient dissolved Fe source. The fraction of dissolved Fe released as Fe(II) from Calbuco ash (~18-38%) was roughly comparable to literature values for Fe released into seawater from aerosols collected over the Pacific Ocean following long range atmospheric transport.

1. Introduction

Volcanic ash has long been considered a large, intermittent source of trace metals to the ocean (Frogner et al., 2001; Sarmiento, 1993; Watson, 1997) and its deposition is now deemed a sporadic generally low-macronutrient, high-micronutrient supply mechanism (Ayris and Delmelle, 2012; Jones and Gislason, 2008; Lin et al., 2011). As volcanic ash can be a regionally significant source of allochthonous inorganic material to affected water bodies, volcanic eruptions have the potential to dramatically change light availability, the carbonate system, properties of sinking particles and ecosystem dynamics (Hoffmann et al., 2012; Newcomb and Flagg, 1983; Stewart et al., 2006). Surveys directly underneath the ash plume from the 2010 eruption of Eyjafjallajökull (Iceland) over the North Atlantic found, among other biogeochemical perturbations, high dissolved Fe (dFe) concentrations of up to 10 nM in affected surface seawater (Achterberg et al., 2013) which could potentially result in enhanced primary production. The greatest potential positive effect of ash deposition on marine productivity would generally be expected in high-nitrate, low-chlorophyll (HNLC) areas of the ocean (Hamme et al., 2010; Mélançon et al., 2014), where low Fe concentrations are a major factor limiting primary production (Martin et al., 1990; Moore et al., 2013). Special interest is therefore placed on the ability of volcanic ash to release dFe, and other bio-essential trace metals such as Mn (Achterberg et al., 2013; Browning et al., 2014; Hoffmann et al., 2012), into seawater. In contrast, apart from inducing light limitation, there are several adverse effects of ash deposition on aquatic organisms. These include metal toxicity (Ermolin et al., 2018), particularly under high dust loading (Hoffmann et al., 2012), and the ingestion of ash particles by filter feeders, phagotrophic organisms or fish (Newcomb and Flagg, 1983; Wolinski et al., 2013). Transient shifts to low pH have also been reported in some, but not all, ash leaching experiments and in some freshwater bodies following

intense ash deposition events, suggesting that significant ash deposition on weakly buffered aquatic environments can also impact and perturb their carbonate system (Duggen et al., 2010; Jones and Gislason, 2008; Newcomb and Flagg, 1983). The greatest negative impact of ash on primary producers would therefore be expected closest to the source where the ash loading is highest and in areas where macronutrients or light, rather than trace elements, limit primary production.

In contrast to the 2010 Eyjafjallajökull plume over the North Atlantic, the 2015 ash plume over the region from the Calbuco eruption (northern Patagonia, Chile) was predominantly deposited over an inshore and coastal region (Romero et al., 2016) (Fig. 1). This led to visible high ash loadings in affected surface waters in the weeks after the eruption (Fig. 2), providing a case study for a concentrated ash deposition event in a coastal system; Reloncaví Fjord, which is the northernmost fjord of Patagonia. It receives the direct discharge from three major rivers, creating a highly stratified and productive fjord system in terms of both phytoplankton biomass and aquaculture production of mussels (González et al., 2010; Molinet et al., 2017; Yevenes et al., 2019). Here we combine in situ observations from moored arrays which were fortuitously deployed in Reloncaví Fjord (Vergara-Jara et al., 2019), with satellite-derived chlorophyll data for offshore regions subject to ash deposition, and leaching experiments carried out on ash collected from the fjord region, to investigate the inorganic consequences of ash addition to natural waters. We thereby evaluate the potential positive and negative effects of ash from the 2015 Calbuco eruption on marine primary production in three geographical regions; Reloncaví Fjord and the areas of the SE Pacific and SW Atlantic Oceans beneath the most intense ash plume.

2. **Materials and methods**

2.1. *Study area*

The Calbuco volcano (Fig. 1) is located in a region with large freshwater reservoirs and in close proximity to Reloncaví Fjord. The predominant bedrock type is andesite (López-Escobar et al., 1995). Reloncaví Fjord is 55 km long and receives freshwater from 3 main rivers, the Puelo, Petrohué, and Cochamó, with mean stream flows of 650 $m^3 s^{-1}$, 350 $m^3 s^{-1}$ and 100 $m^3 s^{-1}$, respectively (León-Muñoz et al., 2013). River discharge strongly influences seasonal patterns of primary production across the region, supplying silicic acid and strongly stratifying the water column (Castillo et al., 2016; González et al., 2010; Torres et al., 2014). Seasonal changes in light availability rather than macronutrient supply are thought to control marine primary production across the Reloncaví region with high marine primary production (>1 g C m^{-2} day^{-1}) throughout austral spring, summer and early autumn (González et al., 2010).

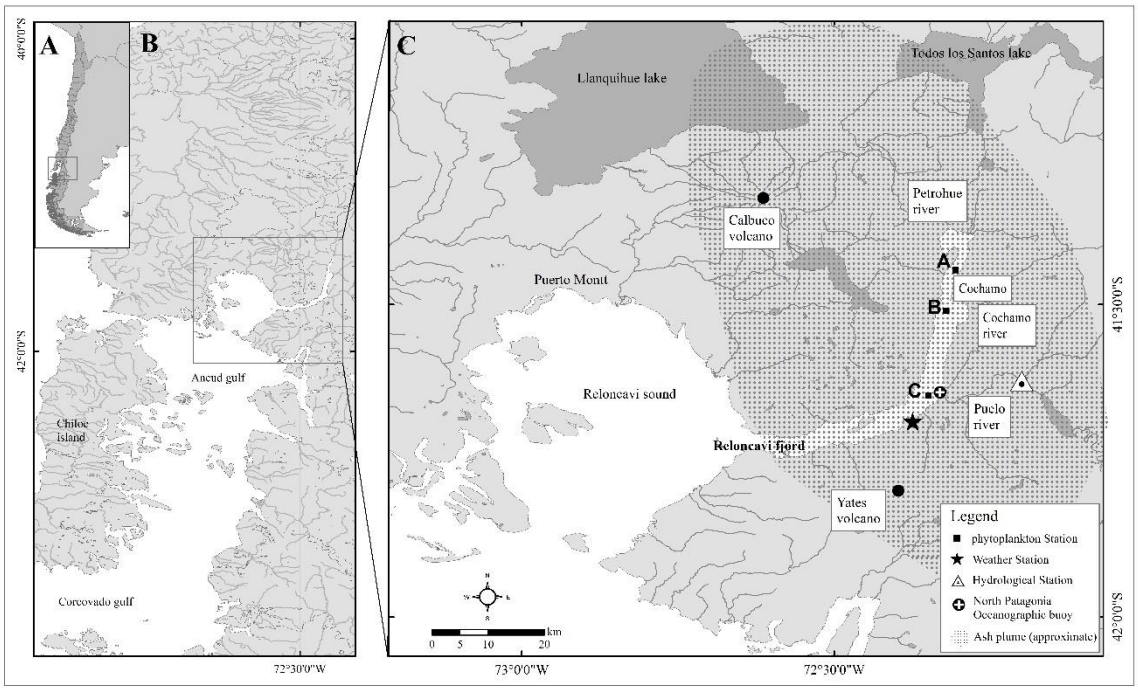

Figure 1. The Calbuco region showing the location of Reloncaví Fjord, 3 major rivers (Petrohué, Cochamó and Puelo) discharging into the fjord, the 3 stations (black squares; A, B and C) used to assess changes in phytoplankton abundance following the eruption, a hydrological station that monitors Puelo river flow, a weather station and the location of a long-term mooring within the fjord. The approximate extent of the ash plume in the week following the first eruption is illustrated, as estimated in technical reports issued by the Servicio Nacional de Geología y Minería (Chile).

On 22 April 2015 the Calbuco volcano erupted after 54 years of dormancy. Two major eruption pulses lasted <2 hours on 22 April and 6 hours on 23 April, releasing a total volume of 0.27 km^3 ash which was projected up to 20 km height above sea level (Van Eaton et al., 2016; Romero et al., 2016). Ash layers of several cm thick were deposited mainly to the NE of the volcano in subsequent days (Romero et al., 2016). A smaller eruption occurred on 30 April projecting ash 4-5 km above sea level which was then mainly deposited south of the volcano. Smaller volumes of ash were released semi-continuously for three weeks after the main eruption, leading to intermittent ash deposition events. Fortuitously, as part of a long-term deployment, an ocean acidification buoy in the middle of Reloncaví Fjord (Vergara-Jara et al., 2019) and an associated meteorological station close to the volcano (Fig. 1) were well placed to assess the impact of ash deposition immediately after the eruption. To complement data from these facilities, after the regional evacuation order was removed, weekly sampling campaigns were conducted in the fjord commencing one week after the eruption. The Chilean Geological-mining Survey (Servicio Nacional de Geología y Minería, SERNAGEOMIN) produced daily technical reports including the estimated area of ash dispersion (http://sitiohistorico.sernageomin.cl/volcan.php?pagina=4&iId=3). This

information was used to create a reference aerial extent of ash deposition for the week after the eruption (Fig. 1, C) and this approximation represents a full week of coverage for this dynamic feature.

2.2. Ash samples – trace metal leaching experiments

On 6 May (2015, Cochamó, Chile, approximately 30 km from the volcano) after the third, and smallest, eruptive pulse of ash from the Calbuco volcano (Fig. 2, A), and with the volcano still emitting material, ash was collected using a plastic tray wrapped with plastic sheeting (40 × 94 cm). The plasticware was left outside for 24 hours until sufficient ash (~500 g) was collected to provide a bulk sample. Ambient weather over the period of ash collection, and the preceding day, was dry (no precipitation). The collected ash was double sealed in low density polyethylene (LDPE) plastic bags and stored in the dark. A sub-sample was analyzed for particle size using a Mastersizer 2000 at The University of Chile.

Ash may affect in situ phytoplankton dynamics in several ways, for example via moderating the carbonate system, macronutrient availability and/or micronutrient availability. As micronutrient (e.g. Fe and Mn) availability is expected to be the main chemical mechanism via which phytoplankton dynamics in the offshore marine environment could be affected, we primarily focus our investigation on the release of dissolved trace metals from ash in seawater. Yet to rule out other potential affects, we also conduct complementary leaches to assess the significance of changes to total alkalinity and macronutrient availability (Table 1). For trace metal leaches, a variety of methods have been used in the literature (Duggen et al., 2010; Witham et al., 2005) depending on the purpose of specific studies. De-ionized water leaches with ash loadings that are high in an offshore environmental context are preferable

for intercomparison studies. The trace metals released under such conditions are however difficult to compare quantitatively to metal exchange processes in the ambient marine environment, especially for elements such as Fe where solubility is strongly influenced by pH, salinity and the nature of dissolved organic carbon present (Baker and Croot, 2010). For prior work conducted specifically using volcanic ash in seawater, 3 main methods have been employed: suspension experiments followed by analysis of the leachate, flow-through reactors, and continuous voltammetric determination of dFe concentrations in situ during suspension experiments (Sup. Table 1). The most commonly used ash:solute ratio in prior seawater experiments is 1:400 (g:mL), with leach lengths varying from 15 minutes to 24 hours (Sup. Table 1). Conversely, incubation experiments designed to test the response of marine phytoplankton to ash deposition have used lower ash:solute ratios of 1:400 to $1:10^7$ which are based on estimates of the ash loading expected to be mixed within the offshore surface mixed layer underneath ash plumes (Browning et al., 2014; Hoffmann et al., 2012). Existing data suggests that ash:solute ratio is not a major factor in determining the release behavior of Fe from ash, however this is acknowledged to be difficult to assess due to other differences between experimental setups used to date (Duggen et al., 2010). Both the age of particles since collection and the organic carbon content of seawater are however known to be critical factors influencing the exchange of Fe, and other trace elements, following any aerosol deposition into seawater (Baker and Croot, 2010; Duggen et al., 2010). Whilst UV-treatment of seawater has been used in some experiments (to remove a large part of any natural organic ligands present, Duggen et al., 2007; Jones and Gislason, 2008), and a strong synthetic organic ligand added in others (to impede dissolved Fe precipitation, Duggen et al., 2007; Olgun et al., 2011; Simonella et al., 2015), to improve reproducibility and standardisation, these steps are not well suited specifically for investigating the release of

206 Fe(II) from ash. Herein we therefore adopt ash:solute ratios comparable to the lower end of
207 the range used in leaching experiments and comparable to the range used in incubation
208 experiments. Seawater was used after prolonged storage in the dark (to reduce biological
209 activity to low background levels) and without UV treatment (to maintain an environmentally
210 relevant level of natural organic material in solution). A short leaching time (10 minutes +
211 filtration) was adopted to minimize bottle effects and recognising that most prior work
212 suggests a large fraction of Fe release occurs on short timescales (minutes), followed by more
213 gradual changes on timescales of hours to days (Duggen et al., 2007; Frogner et al., 2001;
214 Jones and Gislason, 2008).

215 A variety of leaches were conducted in de-ionized water, brackish (fjord) water or offshore
216 South Atlantic seawater (Table 1) with the choice of leaching conditions based on the
217 expected environmental significance in different water masses. Offshore oligotrophic
218 seawater for incubation experiments was collected from an underway transect of the mid-
219 South Atlantic (across 40° S) using a towfish and trace metal clean tubing in a 1 m^3 high
220 density polyethylene tank which had been pre-rinsed with 1 M HCl. This water was stored
221 in the dark for >12 months prior to use in leaching experiments and was filtered
222 (AcroPak1000 capsule 0.8/0.2 µm filters) when subsampling a batch for use in all leaching
223 experiments. All labware for trace metal leaching experiments was pre-cleaned with Mucasol
224 and 1 M HCl. 125 ml LDPE bottles (Nalgene) for trace metal leach experiments were pre-
225 cleaned using a 3-stage procedure with three de-ionized water (Milli-Q, Millipore,
226 conductivity 18.2 MΩ cm^{-1}) rinses after each stage (3 days in Mucasol, 1 week in 1 M HCl,
227 1 week in 1 M HNO_3).

228 Leach experiments were conducted by adding a pre-weighed mass of ash into 100 ml South

229 Atlantic Seawater, gently mixing the suspension for 10 minutes, and then syringe filtering
230 the suspension (0.2 µm, polyvinylidene fluoride, Millipore). Eight different ash loadings
231 from 2-50 mg L^{-1} were used, selected to be environmentally relevant and comparable to prior
232 incubation experiments, with each treatment run in triplicate. Samples for dissolved trace
233 metals (Fe, Cd, Pb, Ni, Cu, Co and Mn) were acidified within 1 day of collection by the
234 addition of 140 µL concentrated HCl (UPA grade, ROMIL) and analysed by inductively
235 coupled plasma mass spectroscopy following preconcentration exactly as per Rapp et al.,
236 (2017).

237 Leach experiments specifically to measure Fe(II) release were conducted in a similar manner
238 but in cold seawater with continuous in-line analysis (5-7°C see Sup. Table 2) due to the
239 rapid oxidation rate of Fe(II) at room temperature (~21°C), which makes accurate
240 measurement of Fe(II) concentrations challenging (Millero et al., 1987). For these
241 experiments, a pre-weighed mass of ash was added to 250 ml South Atlantic seawater and
242 manually shaken for approximately one minute, using an expanded loading range from 0.2-
243 4000 mg L^{-1}. Fe(II) was measured via flow injection analysis using luminol
244 chemiluminescence (Jones et al., 2013) without pre-concentration or filtration. The inflow
245 line feeding the flow injection apparatus was positioned inside the ash suspension
246 immediately after mixing and measurements begun thereafter at 2 minutes resolution.
247 Reported mean values (± standard deviation) are determined from the Fe(II) concentrations
248 measured 2-30 minutes after adding ash into solution. Calibrations were run daily using
249 standard additions of 0.2-10 nM Fe(II) to aged South Atlantic seawater at the same
250 temperature with integrated peak area used to construct calibration curves. Following each
251 leaching experiment the apparatus was rinsed with 0.1 M HCl (reagent grade) followed by

252 flushing with de-ionized water to ensure the removal of ash particles. Blank measurements
253 before/after Fe(II) measurements from experiments with different ash loadings verified that
254 there was no discernable interference from ash particles in the Fe(II) flow-through
255 measurements. Fe(II) leaches were conducted 2 weeks, 4 months and 9 months after the
256 eruption. Fe(II) leaches 2 weeks after the eruption were run for 30 minutes. Fe(II) leaches
257 after 4 or 9 months were run for 1 hour to further investigate the temporal development of
258 Fe(II) concentration. The trace metal leach experiments (above) were conducted at the same
259 time as the first Fe(II) incubation experiments (2 weeks after ash collection).

260 For trace metal leaches, the initial (mean ± standard deviation) dissolved trace metal
261 concentrations were deducted from the final concentrations, in order to calculate the net
262 change as a result of ash addition. For Fe(II) measurements, background levels of Fe(II) were
263 below detection (<0.1 nM) and so no deduction was made.

264 **2.3 Ash samples – de-ionized and brackish water leaching experiments**

265 Fresh brackish sub-surface water from the Patagonia study region was obtained from the
266 Aysén Fjord, at Ensenada Baja (45º21'S: 72º40'W, salinity 16.3), close to the Coyhaique
267 laboratory (Aysén region, Chile) and free from the influence of ash from the 2015 eruption.
268 The oceanographic conditions in these waters are similar to the adjacent Reloncaví fjord
269 (Cáceres et al., 2002). De-ionized water, along with the Aysén fjord brackish water, were
270 used for leaching experiments using two size fractions of ash following the general
271 recommendations of Duggen et al., (2010) and Witham et al., (2005) to consider the effects
272 of different size fractions and leachates. Leaches were conducted in 50 ml LDPE bottles filled
273 with either 40 ml brackish or DI-water with 4 replicates of each treatment. Bottles were

274 incubated inside a mixer at room temperature after the addition of 0.18 g ash, using two ash
275 size fractions (<63 μm and 250-1000 μm) which were separated using sieves (ASTM e-11
276 specification, W.S. Tyler). The mass distribution of the ash as determined by sieving was
277 4.54% >2360 μm; 6.85% <2360 μm and >1000 μm; 31.12% <1000 μm and >250 μm;
278 24.14% <250 μm and >125 μm; 18.04% <125 μm and >63 μm; 15.31% <63 μm. The
279 dominant size fraction by mass was thereby the 250-1000 μm fraction which was analyzed
280 in addition to the finest fraction (<63 μm) with the greatest surface area to mass ratio. The
281 sampling times were at time zero (defined as just after the addition of the ash and a few
282 minutes of mixing), 2 h and 24 h later. Leaching experiments conducted with brackish water
283 were analyzed for total alkalinity (A_T) via a potentiometric titration using reference standards
284 (Haraldsson et al., 1997) ensuring a reproducibility of <2 μmol/kg. For the de-ionized water
285 leaching experiment, A_T was analyzed by titration of unfiltered 5 ml subsamples to a pH 4.5
286 endpoint (Bromocresol Green/Methyl Red) using a Dosimat (Metrohm Inc) and 0.02 N
287 H_2SO_4 titrant. Alkalinity was calculated as $CaCO_3$ equivalents following APHA (American
288 Public Health Association) 2005-Methods 2320 (2320 Alkalinity, titration method).
289 Additional 5 ml subsamples were filtered, stored at 4°C and analyzed within 3 days for major
290 ions (F^-, Cl^-, SO_4^{2-}, NO_3^-, Li^+, Na^+, NH_4^+, K^+, Mg^{2+}, Ca^{2+}) using a DionexTM 5000 Ion
291 Chromatography system with Eluent Generation (APHA). All measurements were then
292 corrected for initial water concentrations prior to ash addition. Saturation indices for species
293 in solution following leaching from <63 μm ash particles were obtained from the MINTEQ
294 3.1. IAP Ion Activity Product chemical equilibrium model (see Sup. Table 6).

295 Table 1. Summary of different leaching experiments and samples.

Ash/ particle source	De-ionized water leaches	Brackish (fjord) water	South Atlantic seawater	Nº of replicates
Calbuco ash, sieved <63 μm	Total alkalinity, ion and macronutrients	Total alkalinity	-	4
Calbuco ash, sieved 250-1000 μm	Total alkalinity, ion and macronutrients	Total alkalinity	-	4
Calbuco ash, unsieved	-	-	Trace metals, Fe(II)	3 for trace elements, 1 time series for Fe(II)

2.4 Environmental data – continuous Reloncaví Fjord monitoring

High temporal resolution (hourly) in situ measurements were taken in the Reloncaví fjord (Fig. 1 C, North Patagonia Oceanographic Buoy) at 3 m depth using SAMI sensors that measured spectrophotometric CO_2 and pH (DeGrandpre et al., 1995; Seidel et al., 2008) (Sunburst Sensors, LLC), and an SBE 37 MicroCAT CTD-ODO (SeaBird Electronics) for temperature, conductivity, depth and dissolved O_2, as per Vergara-Jara et al., (2019). Sensor maintenance and quality control is described by Vergara-Jara et al., (2019). The error in pCO_2 concentrations is estimated to be at most 5% which arises mainly due to a non-linear sensor response and reduced sensitivity at high pCO_2 levels >1500 ppm (DeGrandpre et al., 1999). The SAMI-pH instruments used an accuracy test instead of a calibration procedure (Seidel et al., 2008). With the broad pH and salinity range found in the fjord, pH values are subject to a maximum error of ±0.02 (Mosley et al., 2004).

A meteorological station (HOBO-U30, Fig. 1) measured air temperature, solar radiation,

wind speed and direction, rainfall, and barometric pressure every 5 minutes. Puelo River streamflow was obtained from the Carrera Basilio hydrological station (Fig. 1), run by Dirección General de Aguas de Chile (http://snia.dga.cl/BNAConsultas/reportes).

2.5 Field surveys in Reloncaví Fjord post eruption

During May 2015, weekly field campaigns were undertaken in the Reloncaví Fjord. Phytoplankton samples were collected at 3 depths (1 m, 5 m and 10 m) for taxonomic characterization and abundance determination at 3 stations (A, B and C; Fig. 1) using a 5 L Go-Flo bottle. Samples were analyzed using an Olympus CKX41 inverted phase contrast microscope using a 10 ml sedimentation chamber and the Utermöhl method (Utermöhl, 1958). The phytoplankton community composition was then statistically analyzed in R (RStudio V 1.2.5033) using general linear models in order to find statistically significant differences between dates and group abundances. Additionally, as part of a long-term monitoring program at station C (Fig. 1), chlorophyll-a samples were retained from 6 depths (1, 3, 5, 7, 10 and 15 m) on 6 occasions during March-May 2015. Chlorophyll-a was determined by fluorometry after filtering 250 ml of sampled water through GFF filters (Whatman) as per Welschmeyer (1994). Two additional profiles close to Station C were obtained from Yevenes et al., (2019). Integrated chlorophyll-a (mg m^{-2}) and diatom abundance (cells m^{-2}) were determined to 15 m depth. Chlorophyll-a within Reloncaví Fjord is invariably concentrated in the upper ~10 m (González et al., 2010; Yevenes et al., 2019) and thus, for comparison to prior reported data integrated to 10 m, only a small difference is anticipated. For all profiles considered herein, there is a 20% difference between integrating to 10 m or 15 m depth.

2.6 Satellite data

Daily, 4 km resolution chlorophyll-a images from the MODIS Aqua sensor (OCI algorithm; Hu et al., 2012) were downloaded from the NASA Ocean Color website (https://oceancolor.gsfc.nasa.gov) for the period 4 April 2015–2 May 2015. As the UV Aerosol Index largely reflects strongly UV-absorbing (dust) aerosols (Torres et al., 2007), this was used as a proxy for the spatial extent and loading of the ash plume. The UV aerosol index product from the Ozone Monitoring Instrument (OMI) on the EOS-Aura was downloaded for the same time period. Daily images were composited into 5-day mean averages.

3. Results

3.1 In situ observations

The Calbuco ash plume reached up to 20 km height and was dispersed hundreds of kilometers across Patagonia and the Pacific and Atlantic Oceans (Fig. 2) (Van Eaton et al., 2016; Reckziegel et al., 2016; Romero et al., 2016). The ash loading in water bodies near the cone was visually observed to be high, especially near the Petrohué river catchment that drains into the head of the Reloncaví fjord. This ash loading into the fjord was clearly visible on 6 May 2015 when ash samples were collected for leaching experiments (Fig. 2).

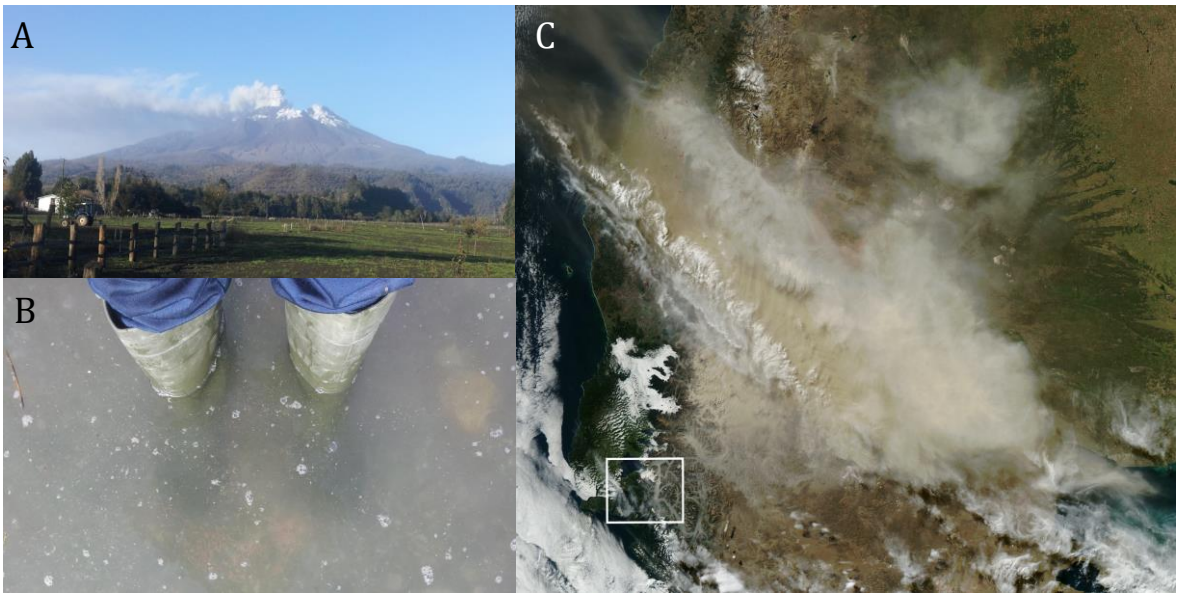

Figure 2. A Calbuco volcano ash plume 6 May 2015. B Reloncaví Fjord water with atypical high turbidity due to the ash loading, Cochamó town 6 May. C Ash cloud visible on MODIS Aqua satellite from the NASA Earth Observatory, 23 April (http://earthobservatory.nasa.gov/NaturalHazards/view.php?id=85767&eocn=home&eoci=nh). The highlighted box in C corresponds to Fig. 1 C.

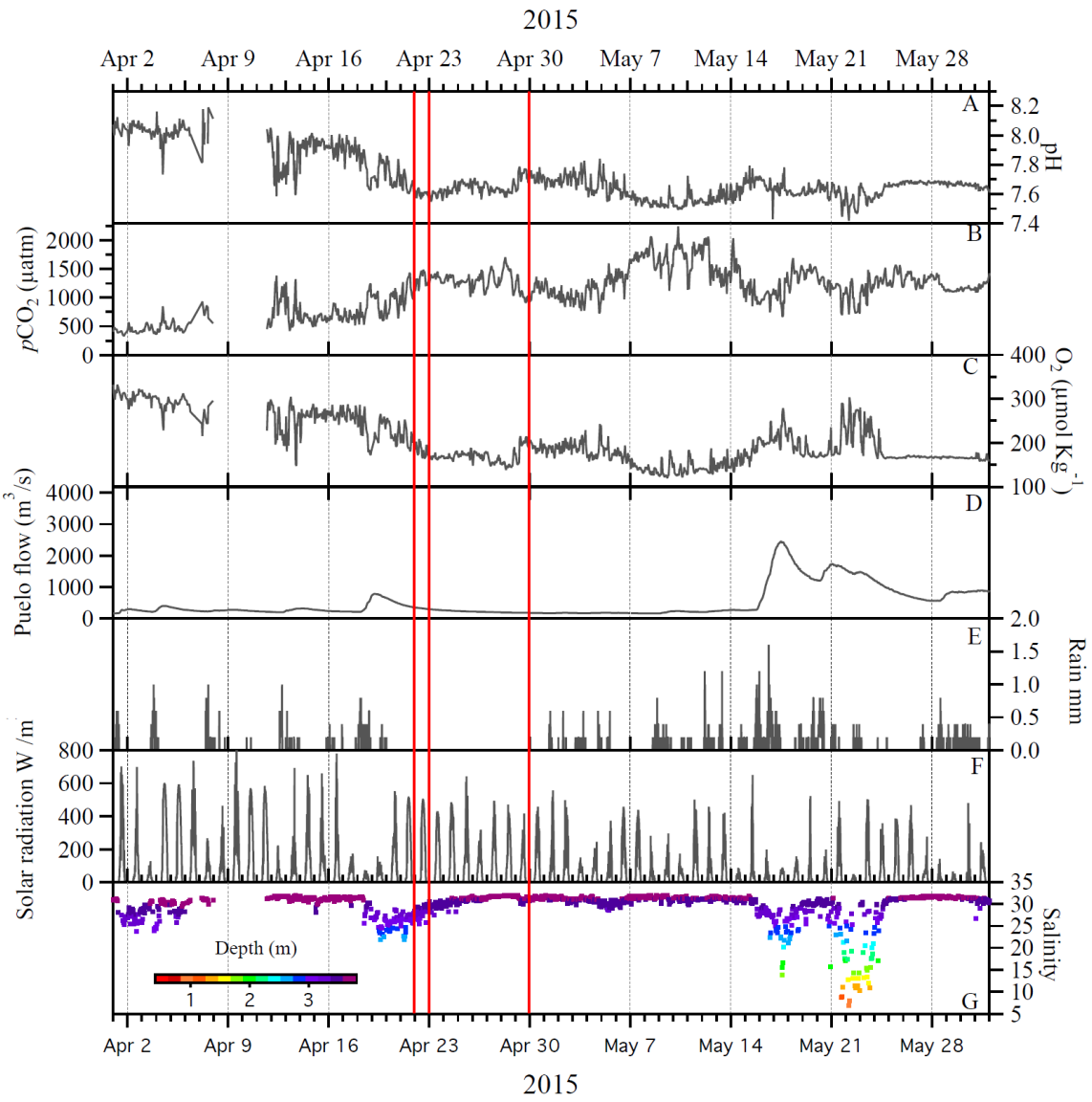

354

355 Figure 3. Continuous data from the Reloncaví Fjord mooring and nearby hydrological and
356 weather stations for April-May 2015. The vertical red lines mark the eruption dates. All
357 locations are marked in Fig 1. Carbonate chemistry and salinity data from Vergara-Jara et
358 al., (2019). Wind and tidal mixing caused small changes in the depth of the sensors which
359 are shown alongside the salinity data.

360

Carbonate chemistry data from the Reloncaví Fjord mooring demonstrated that pH declined and pCO_2 increased in the week prior to the first eruption (22 April, Fig. 3). Oxygen and pH reached a minimum and pCO_2 a maximum during the time period 7-14 May, which indicates a state of high respiration. In this stratified environment, the brackish fjord surface layer has generally low pH, high pCO_2 with seasonal changes in salinity and respiration leading to a large annual range of pCO_2 and pH (Vergara-Jara et al., 2019). The depth of the sensors varied temporally due to changes in tides and river flow. This accounts for some of the variation in measured salinity due to the strong salinity gradient with depth in the brackish surface waters (Fig. 3). Any changes to pCO_2 or pH occurring as a direct result of the eruptions, or associated ash deposition, are therefore challenging to distinguish from background variation due to short-term (intra-day) or seasonal shifts in the carbonate system which are pronounced in this dynamic and strongly freshwater influenced environment (Fig. 3). Freshwater discharge from the Puelo increased sharply from 16 May which is an annually recurring event (González et al., 2010).

3.2 Phytoplankton in Reloncaví fjord post-eruption

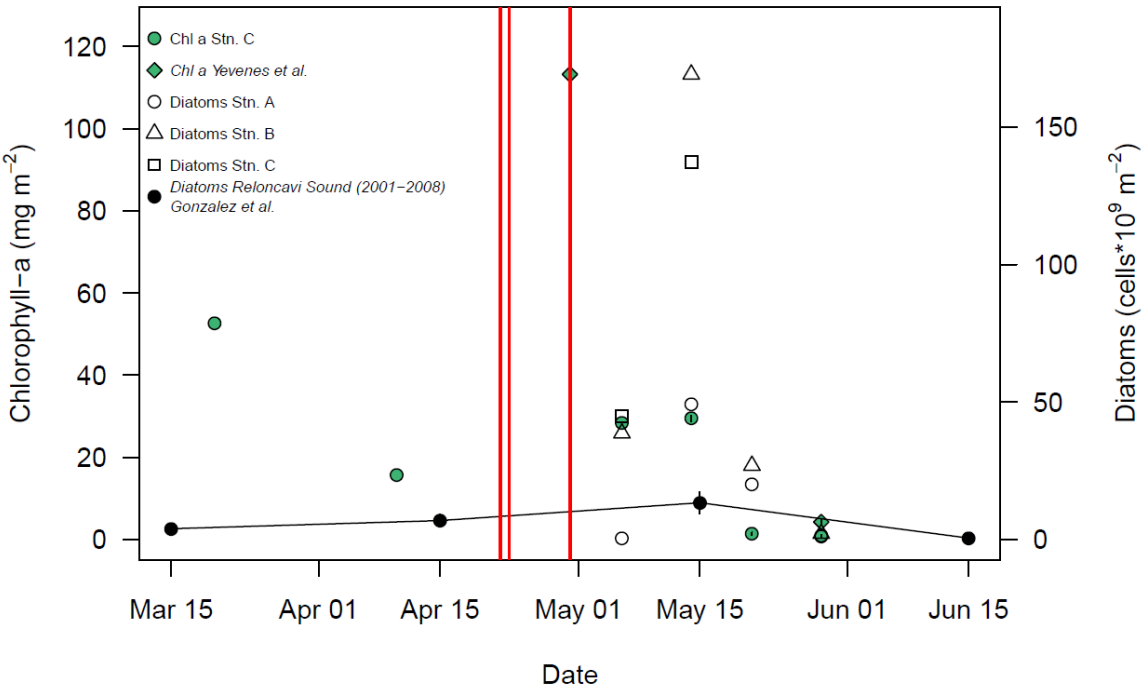

376

377 Figure 4. Changes in integrated (0-15 m) diatom abundance and chlorophyll-a for Reloncaví
378 Fjord in April-May 2015. Locations as per Fig. 1, the eruption dates are marked with red
379 lines. Historical diatom data from Reloncaví Sound (2001-2008, integrated to 10 m depth,
380 mean ± standard error, González et al., 2010) and additional chlorophyll data from 2015
381 ('Station 3' from Yevenes et al., 2019, approximately corresponding to Station C herein) are
382 also shown.

383

384 Phytoplankton abundances observed in May 2015 within Reloncaví Fjord were assessed by
385 diatom cell counts and chlorophyll-a concentrations (Sup. Table 3) and were proportionate
386 to, or higher than, those previously observed in the region (Fig. 4). When comparing
387 observations to prior data from González et al., (2010) it should be noted that there is a slight
388 depth discrepancy (earlier work was integrated to 10 m depth rather than 15 m herein). Yet
389 as the phytoplankton bloom is overwhelmingly present within the upper 10 m these data do

provide a useful comparison. Diatom abundance integrated to 15 m depth peaked at Stations B and C around 14 May, with notably lower abundances at the innermost station A (Fig. 4). The highest measured chlorophyll-a concentrations were on 30 April at Station C, then chlorophyll-a values declined to much lower concentrations in late May which is expected from patterns in regional primary production (González et al., 2010). No measurements were available for 10-30 April 2015 (Fig. 4) and thus it is not possible to determine the timing of the onset of the austral autumn phytoplankton bloom with respect to the volcanic eruptions from the available chlorophyll-a or diatom data. Within this time period, the mooring at Station C (Fig. 3) however did record a modest increase in pH and O_2 from 28-29 April, during a time period when river discharge and salinity were stable, which could be indicative of the autumn phytoplankton bloom onset.

3.3 Total alkalinity and macronutrients in leach experiments

Size analysis of the collected ash determined a mean particle diameter of 339 µm. Small ash-particles (<63 µm) resulted in minor, or no significant, changes to A_T in brackish fjord waters (Fig. 5). With larger ash-particles (250-1000 µm) no effect was evident. Conversely, a leaching experiment with de-ionized water showed a small increase in A_T (Fig. 5) for both size fractions. By increasing the A_T of freshwater, ash would act to increase the buffering capacity of river outflow into a typically weak carbonate system like the Reloncaví Fjord (Vergara-Jara et al., 2019). However, the absolute change in A_T was relatively small despite the large ash loading used in all incubations (< 20 µmol kg^{-1} A_T for ash loading >4 g L^{-1}) and therefore it is expected that the direct effect of ash on A_T in situ was limited. Other effects on carbonate chemistry may however arise due to ash moderating the timing and intensity of primary production and thus biological pCO_2 drawdown.

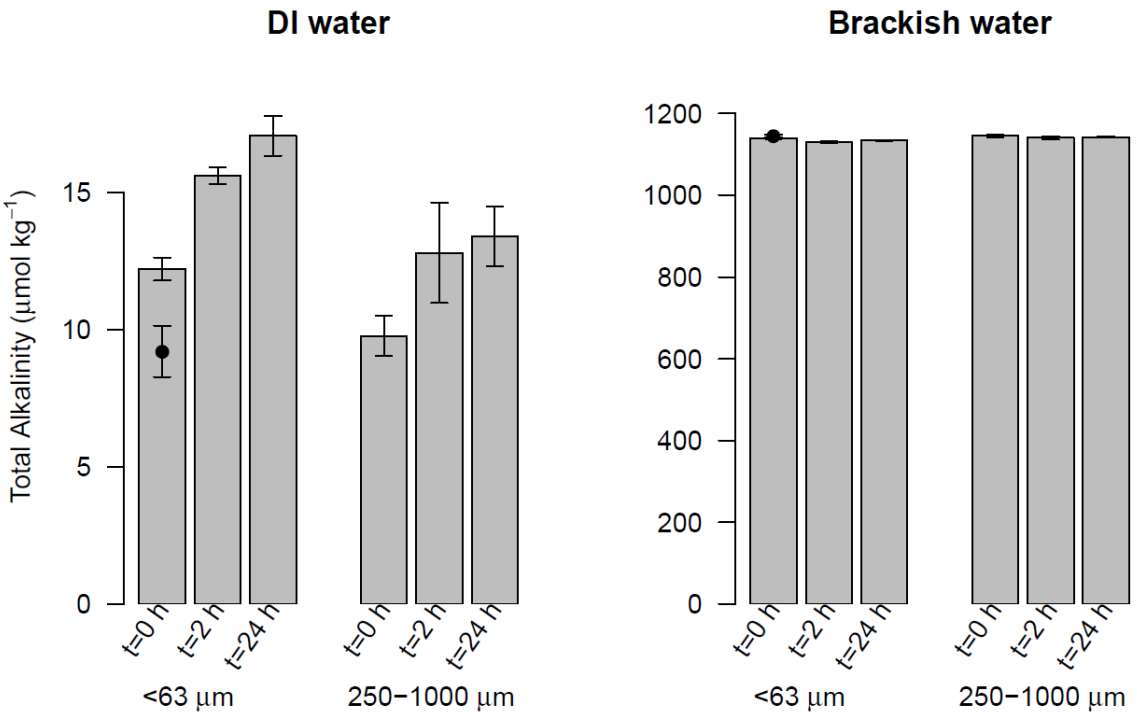

414

415 Figure 5. Total alkalinity released after leaching 4.5 g L^{-1} ash of two size fractions (<63 µm
416 and 250-1000 µm) in de-ionized water (DI water) and brackish water. T_0= 'time zero',
417 measured after one minute of mixing, T_{2H}= after two hours of mixing, T_{24H}= after 24 hours
418 of mixing. n=4 for all treatments (mean ± standard deviation plotted). The initial (pre-ash
419 addition) alkalinity is marked by a black dot superimposed on the left T_0. Source data is
420 provided in Supplementary Table 4.

421

422 Ion chromatography results for Na^+, K^+, Ca^{2+}, F^-, Cl^-, NO_3^- and SO_4^{2-} showed that in the
423 presence of smaller ash size particles, ion inputs were generally higher (Table 2) as has been
424 reported previously (Jones and Gislason, 2008; Óskarsson, 1980; Rubin et al., 1994). The
425 leaching from ash components into de-ionized water occurred almost instantly with limited,
426 or no increases in leached concentrations observed between 0, 2 and 24 h (Table 2). For larger
427 particles there was less release of most ions. In the case of Ca^{2+} and SO_4^{2-} a more gradual

leaching effect was apparent (Table 2). The concentrations of NO_3^- and NH_4^+ were generally below detection suggesting that ash was a minor source of fixed-nitrogen into solution. These observations are consistent with the trends in prior work using a range of volcanic ash and incubation conditions (Duggen et al., 2010; Witham et al., 2005). Major ion analysis was only conducted in de-ionized water as no significant changes would be observable for most of these ions in brackish or saline waters under the same conditions.

	Time [h]	**Na^+**	**K^+**	**Ca^{2+}**	**F^-**	**Cl^-**	**SO_4^{2-}**	**NO_3^-**	**NH_4^+**
Detection limit		*0.17*	*0.43*	*0.30*	*0.28*	*1.31*	*1.64*	*0.34*	*0.13*
Proced. Blank		b.d.	b.d.	0.39	b.d.	b.d.	b.d.	b.d.	b.d.
250-1000 µm [µmol/l]	0.1	3.4 (2.8)	0.83 (0.3)	18.3 (3.3)	0.16 (0.05)	3.7 (1.9)	3.7 (2.2)	b.d.	0.15 (0.2)
	2	5.1 (2.0)	1.0 (0.2)	18.5 (4.5)	0.21 (0.08)	4.4 (1.6)	4.9 (2.0)	b.d.	0.38 (0.4)
	24	7.3 (0.1)	1.4 (0.2)	23.4 (3.2)	0.52 (0.18)	5.7 (0.5)	8.3 (2.1)	b.d.	b.d.
<63 µm [µmol/l]	0.1	16.2 (12.7)	3.2 (0.3)	25.1 (5.4)	0.29 (0.0)	17.1 (13.6)	13.5 (1.3)	0.53 (0.2)	1.70 (1.1)
	2	16.7 (1.0)	3.8 (0.1)	31.8 (2.7)	0.63 (0.2)	15.2 (0.9)	19.0 (0.3)	b.d.	0.52 (1.0)
	24	17.3 (0.8)	3.9 (0.3)	33.8 (3.3)	0.69 (0.3)	14.6 (1.0)	18.8 (0.5)	b.d.	1.32 (2.6)
<63 µm [µmol/g ash]	24	3.84	0.87	7.50	0.15	3.25	4.18	0.048	0.29
	Range (lit.)	1.5-84.3	0.1-5.4	0.6-589	0.1-9	2-92.9	1-554	0-6.4	0.3-0.6

Table 2. Major ion and macronutrient concentrations in µmol/l leached from the two size fractions of ash (< 63 µm and 250-1000 µm) into deionized water (b.d. = below detection). Shown are mean, with standard deviation in parentheses (n=4). Also shown are mass normalized values [µmol/g ash], and a comparison to the range of values reported by Jones and Gislason (2008).

3.4 Trace elements in leach experiments

Release of nanomolar concentrations of dissolved Fe and Mn was evident when ash was re-suspended in aged seawater for 10 minutes (Fig. 6). The net release of dissolved metals proceeded with varying relationships with ash loading over the applied gradient (2-50 mg L^-

444 [1]). Dissolved Mn, Pb, Cu and Co release exhibited significant ($p < 0.05$) positive relationships
445 with ash loading, with Mn and Cu exhibiting the most linear behavior (R^2 0.99 and 0.83,
446 respectively). Dissolved Fe, Cd and Ni showed no significant relationships with ash loading
447 over the applied range. The initial concentration of metals in South Atlantic seawater should
448 however also be considered when interpreting the trends. The magnitude of changes in Cd
449 and Ni concentrations were smallest relative to both the initial concentration and the standard
450 deviation on the initial concentration (0.38 ± 0.04 nM Cd and 6.58 ± 0.76 nM Ni,
451 respectively). It thus would be difficult to extract a clear relationship irrespective of their
452 chemical behavior. For other elements (Fe, Co and Pb), non-linearity between ash addition
453 and trace metal concentrations, and some negative changes in concentrations, both likely
454 reflect scavenging of metal ions onto ash particle surfaces (Rogan et al., 2016). Fe, Co and
455 Pb are all scavenged type elements and so increasing the surface area of ash present may
456 affect the net change in metal concentration. The divergence between the behaviour of Mn
457 and Fe, with Mn showing a stronger relationship with ash loading, supports the hypothesis
458 of Mendez et al., (2010), that the release of dissolved Mn from aerosols into seawater depends
459 primarily on ash Mn availability whereas the release of dissolved Fe is more dependent on
460 the nature of organic material present in solution.

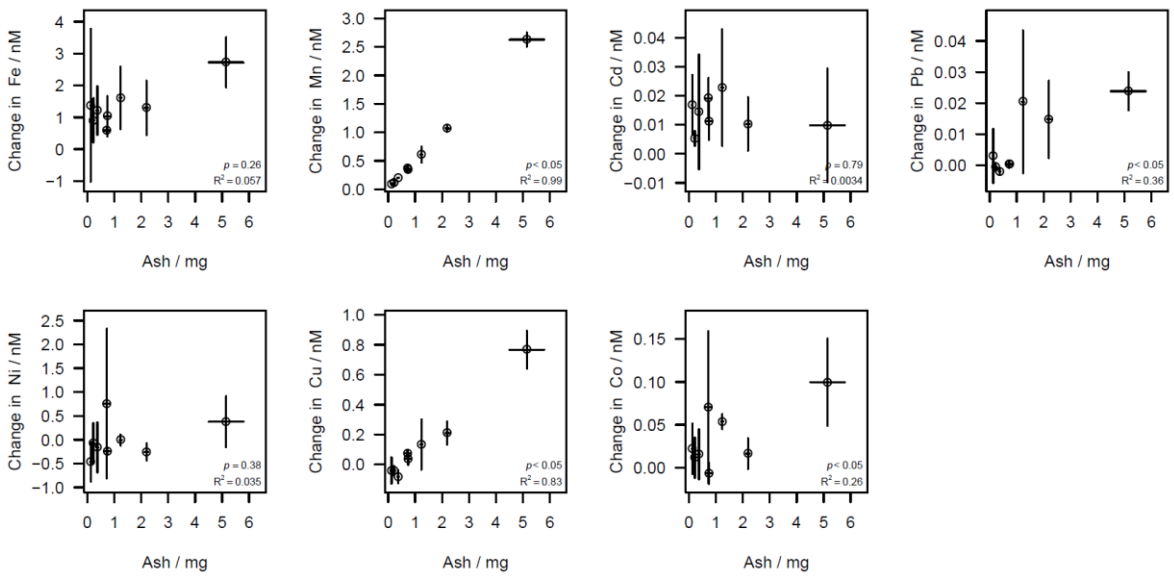

Figure 6. Change in trace metal concentrations after varying ash addition to 100 ml South Atlantic seawater for a 10-minute leach duration at room temperature. Initial (mean ± standard deviation) dissolved trace metal concentrations - deducted from the final concentrations to calculate the change as a result of ash addition - were 0.98 ± 0.03 nM Fe, 0.38 ± 0.04 nM Cd, 13 ± 2 pM Pb, 6.58 ± 0.76 nM Ni, 0.84 ± 0.07 nM Cu, 145 ± 9 pM Co, 0.72 ± 0.05 nM Mn. Error bars are standard deviations from triplicate treatments with similar ash loadings. p values and R^2 for a linear regression are annotated. Source data is provided in Supplementary Table 5. The same data with individual replicates is shown in Supplementary Figure 1.

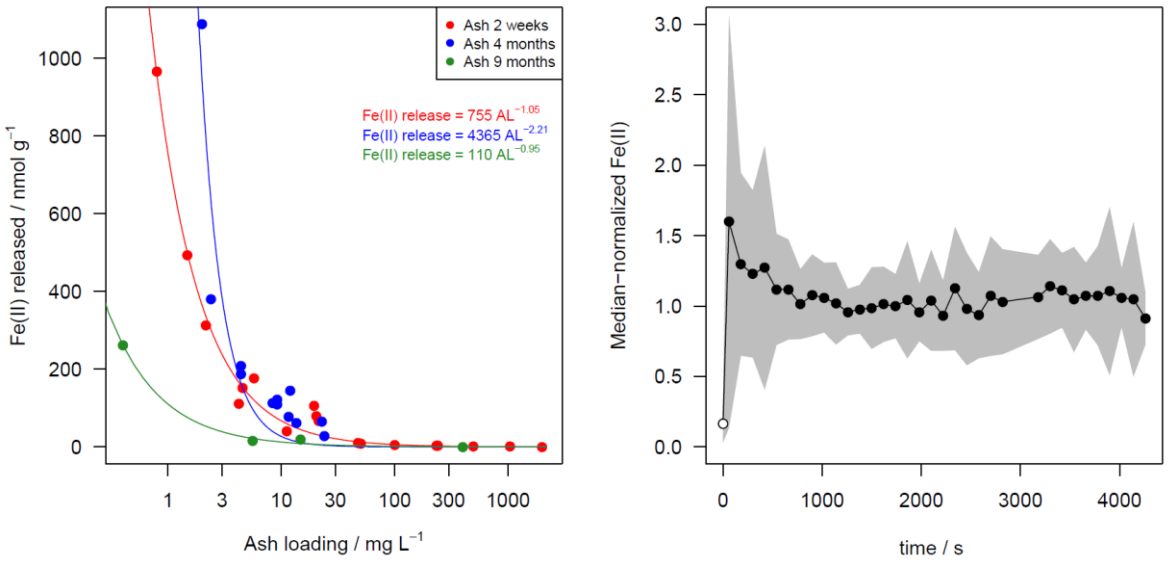

471

472 Figure 7. Fe(II) release from Calbuco ash into seawater. Mean Fe(II) released into South
473 Atlantic seawater over a 30 minute leach at 5-7°C (left). The same batch of Calbuco ash was
474 subsampled and used to conduct experiments on 3 occasions after the 2015 eruption (2 weeks,
475 4 months and 9 months since ash collection). The lines are power law fits, with associated
476 equations shown in the legend. The 3 time-series of Fe(II) concentrations following ash
477 addition is considered collectively by normalizing the measured concentrations (right), such
478 that 1.0 represents the median Fe(II) concentration measured in each experiment. All
479 experiments were conducted for at least 30 minutes, those conducted with 4/9 months old
480 ash were extended for 1 hour. The black line shows the mean response over 34 leach
481 experiments with varying ash loading, the shaded area shows ± 1 standard deviation. The
482 initial Fe(II) concentration (pre-ash addition at 0 s) in all cases was below detection and thus
483 the detection limit is plotted at 0 s (open circle). Source data is provided in Supplementary
484 Table 2.

485

In addition to the release of dFe in solution, which generally exists as Fe(III) species in oxic seawater (Gledhill and Buck, 2012), the release of Fe(II) was evident on a similar timescale when cold (5-7°C) aged S Atlantic seawater was used as leachate (Fig. 7). The half-life of Fe(II) decreases more than tenfold as temperature is increased from 5 to 25°C, leading to Fe(II) decay on timescales shorter than the time required for analysis (approximately 60 s for solution to enter the flow injection apparatus, mix with reagent and generate a peak) (Santana-Casiano et al., 2005). Elevated Fe(II) concentrations (mean 0.8 nM, Sup. Table 2) were evident at this temperature (5-7°C), which represents an intermediate sea surface temperature for the high latitude ocean. A sharp decline in Fe(II) dissolution efficiency with increasing ash load was also evident (Fig. 7). Both the highest Fe(II) concentration and the highest net release of Fe(II) were observed at the lowest ash loading (Fig. 7 and Sup. Fig. 2). Fe(II) concentration following dust addition into seawater was possibly reduced when the same experimental leaches with ash were repeated 9 months after the initial experiment. The first leaches were conducted ~2 weeks after ash collection. The absence of a clear change between 2 weeks and 4 months precludes an accurate assessment of the rate at which Fe(II) solubility may have decreased.

As Fe(II) concentrations were measured continuously using flow injection analysis, the temporal development of Fe(II) concentration after ash addition to cold seawater can also be shown (Fig. 7). Considering the set of leach experiments collectively, all ash additions were characterized by a sharp increase in Fe(II) concentrations in the first minute after ash addition into seawater. This was typically followed by a decline and then a relatively stable Fe(II) concentration (Fig. 7).

3.5 Satellite observations

Five-day composite images of atmospheric aerosol loading (UV aerosol index, which largely represents strongly UV-absorbing dust, Torres et al., 2007) indicated two main volcanic eruption plume trajectories following the major eruptions on 22 and 23 April: (i) northwards over the Pacific, and (ii) northeast over the Atlantic. Daily resolved time series were constructed for regions in the Atlantic and Pacific with elevated atmospheric aerosol loading (UV Aerosol Index ~2 a.u.; Fig. 8). The Pacific time series indicated a pronounced peak in aerosol index followed by chlorophyll-a one day later. A control region to the south of the ash-impacted Pacific region showed no clear changes in chlorophyll-a matching that observed in the higher UV aerosol index region to the north (Sup. Fig. 3).

Conversely, in the Atlantic, where the background chlorophyll-a concentration was higher throughout the time period of interest, the main area with enhanced aerosol index was not clearly associated with a change in chlorophyll-a dynamics on a timescale comparable to that observed following other volcanic ash fertilized events (Fig. 8). In a smaller ash impacted area to the south of the Rio de la Plata (Sup. Fig. 3), where nitrate levels are expected to be higher than to the north and Fe levels also expected to be elevated due its location on the continental shelf, a chlorophyll-a peak was evident 7 days after the UV aerosol peak. However, this was not well constrained due to poor satellite coverage in the period after the eruption.

Prior eruptions have been attributed with driving time periods of enhanced regional marine primary production beginning 3-5 days post-eruption (Hamme et al., 2010; Langmann et al., 2010; Lin et al., 2011) and bottle experiments showing positive chlorophyll changes in

533 response to ash addition are typically significant compared to controls within 1-4 days
534 following ash addition (Browning et al., 2014; Duggen et al., 2007; Mélançon et al., 2014).

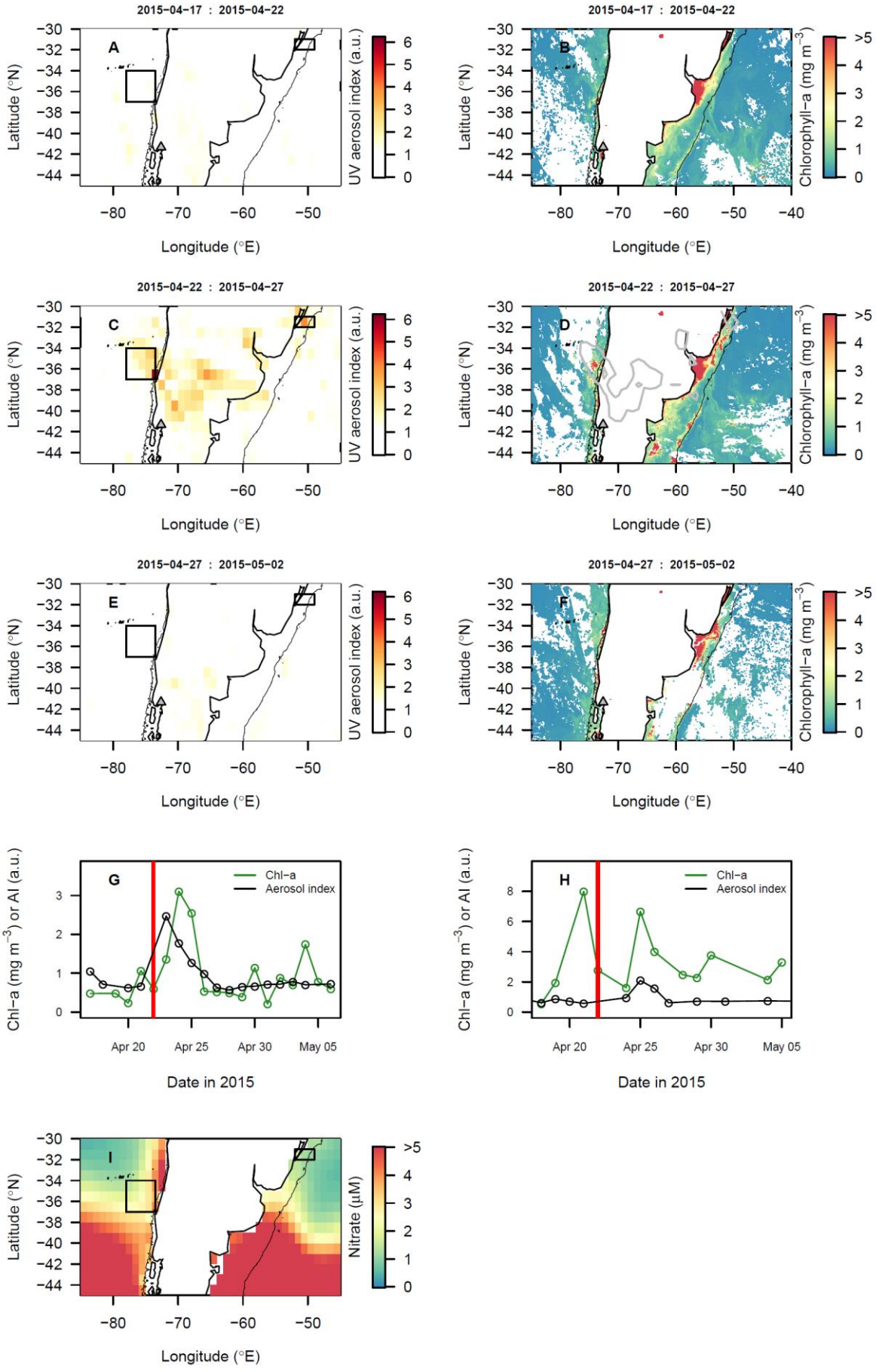
2015-04-17 : 2015-04-22
A
B
2015-04-22 : 2015-04-27
C
D
2015-04-27 : 2015-05-02
E
F
Latitude (°N)
Longitude (°E)
UV aerosol index (a.u.)
Chlorophyll-a (mg m^{-3})
G
H
Chl-a
Aerosol index
Chl-a (mg m^{-3}) or AI (a.u.)
Apr 20
Apr 25
Apr 30
May 05
Date in 2015
I
Nitrate (µM)

Figure 8. Potential biological impact of the 2015 Calbuco eruption observed via satellite remote sensing. (A-F) Spatial maps showing the distribution of ash in the atmosphere (UV Aerosol Index) and corresponding images of chlorophyll-a. Images were composited over 5-day periods. Grey lines in chlorophyll maps corresponds to the UV Aerosol index = 2 a.u. contour. (G, H) Time series of UV Aerosol Index and chlorophyll-a for regions of the Pacific (G) and Atlantic (H) identified by boxes in maps. Red vertical lines (22 April) indicate the first eruption date. (I) Mean World Ocean Atlas surface NO_3 concentrations. Thin black lines indicate the 500 m bathymetric depth contour.

4 Discussion

4.1 Local drivers of 2015 bloom dynamics in Reloncaví Fjord

The north Patagonian archipelago and fjord region have a seasonal phytoplankton bloom cycle with peaks in productivity occurring in May and October (austral autumn and spring) and the lowest productivity consistently in June (austral winter)(González et al., 2010). Diatoms normally dominate the phytoplankton community during the productive period due to high light availability and high silicic acid supply, both of which are influenced by freshwater runoff (González et al., 2010; Torres et al., 2014). The austral fall season, encompassing the April-May 2015 ash deposition events, is therefore expected to have a high phytoplankton biomass (Iriarte et al., 2007; León-Muñoz et al., 2018) which terminates abruptly with decreasing light availability in austral winter (González et al., 2010).

Whilst not directly comparable, the magnitude of the 2015 bloom in terms of diatom abundance (Fig. 4) was more intense than that reported in Reloncaví Sound 2001-2008. With respect to the timing of the phytoplankton bloom, the low diatom abundances and

chlorophyll-a concentrations at the end of May (Fig. 4) are consistent with prior observations of sharp declines in primary production moving into June (González et al., 2010). Peaks in diatom abundance were measured at two stations on 14 May one week after the third (small) eruptive pulse, and measured chlorophyll-a concentrations were highest close to Station C on 30 April (Fig. 4). The high-resolution pH and O_2 data collected at Station C from mooring data is consistent with an intense phytoplankton bloom between ~29 April and 7 May (Fig. 3) indicated by a shift to slightly higher pH and O_2 during this time period when river flow into the fjord was stable.

Without a direct measure of ash deposition per unit area in the fjord, turbidity, or higher resolution chlorophyll/diatom data, it is challenging to unambiguously determine the extent to which the austral autumn phytoplankton bloom was affected by volcanic activity. The high abundance of diatoms at two of three stations sampled could have resulted from ash fertilization. Yet if this was the case, it is not clear which nutrient was responsible for this fertilization, why the bloom initiation occurred about one week after the third eruptive pulse (several weeks after the main eruption events) and to what extent the timing was coincidental given that productivity normally peaks in May. Reloncaví Fjord was to the south of the dominant ash deposition from the 22 and 23 April eruptions (Romero et al., 2016) and thus ash was delivered by a mixture of vectors including runoff and rainfall. The Petrohue river basin was particularly severely affected by ash with deposition of up to 50 cm ash in places. This complicates the interpretation of the time series provided by high resolution data (Fig. 3). With incident light also highly variable over the time series (Fig. 3F), there are clearly several factors, other than volcanic ash deposition, which will have exerted some influence on diatom and chlorophyll-a abundance throughout May 2015.

Primary production in the Reloncaví region is thought to be limited by light availability rather than macronutrient availability (González et al., 2010). Whilst micronutrient availability relative to phytoplankton demand has not been extensively assessed in this fjord, with such higher riverine inputs across the region- which are normally a large source of dissolved trace elements into coastal waters (e.g. Boyle et al., 1977)- limitation of phytoplankton growth by Fe, or another micronutrient, seems implausible. Reported Fe concentrations determined by a diffusive gel technique in Reloncaví Fjord in October 2006 were relatively high; 46-530 nM (Ahumada et al., 2011). Similarly, reported dFe concentrations in the adjacent Comau Fjord at higher salinity are generally in the nanomolar range and remain >2 nM even under post-bloom conditions which suggests dFe is not a limiting factor for phytoplankton growth (Hopwood et al., 2020; Sanchez et al., 2019).

Silicic acid availability could have been increased by ash deposition. Whilst not quantified herein, an increase in silicic acid availability from ash in a region where silicic acid was sub-optimal for diatom growth could plausibly explain higher than usual diatom abundance (Siringan et al., 2018). Silicic acid concentrations were indeed high (up to 118 µM) in Reloncaví Fjord surface waters and >30 µM at 15 m depth (salinity 33.4) (Vergara-Jara et al., 2019; Yevenes et al., 2019). However concentrations >30 µM are typical during periods of high runoff and accordingly are not thought to limit primary production or diatom growth in this area (González et al., 2010). The $Si(OH)_4$:NO_3 ratio in Reloncaví Fjord and downstream Reloncaví Sound also indicates an excess of $Si(OH)_4$, with ratios of approximately 2:1 observed in fjord surface waters throughout the year (González et al., 2010; Yevenes et al., 2019). For comparison, the ratio of Si:N for diatom nutrient uptake is

608 15:16 (Brzezinski, 1985). Furthermore, experimental incubations making additions of
609 macronutrients to fjord waters in Reloncaví and adjacent fjords, have found strong responses
610 of phytoplankton to additions of silicic acid only when $Si(OH)_4$ and NO_3 were added in
611 combination, further corroborating the hypothesis that an excess of silicic acid is normally
612 present in surface waters of these fjord systems (Labbé-Ibáñez et al., 2015). It is therefore
613 doubtful that changes in nutrient availability from ash alone could explain such high diatom
614 abundances in mid-May.
615
616 Alternative reasons for high diatom abundances in the absence of a chemical fertilization
617 effect are plausible and could include, for example, ash having reduced zooplankton
618 abundance or virus activity in the fjord, thus facilitating higher diatom abundance than would
619 otherwise have been observed by decreasing diatom mortality rates in an environment where
620 nutrients were replete. The role of volcanic ash in driving such short-term ecological shifts
621 in the marine environment is almost entirely unstudied (Weinbauer et al., 2017). However,
622 volcanic ash deposition of 7 mg L^{-1} in lakes within this region during the 2011 Puyehue-
623 Cordón Caulle eruption was reported to increase post-deposition phytoplankton biomass and
624 decrease copepod and cladoceran biomass (Wolinski et al., 2013). The proposed mechanism
625 was ash particle ingestion negatively affecting zooplankton, and ash-shading positively
626 affecting phytoplankton via reduced photoinhibition (Balseiro et al., 2014; Wolinski et al.,
627 2013).
628
629 Considering the more modest peak in diatom abundance at the most strongly ash affected
630 station (Station A, Fig. 4) and the timing of the peak diatom abundance 3 weeks after the
631 main eruption, it is clear that the interaction between ash and phytoplankton in the Reloncaví

Fjord was more complex than the simple Fe-fertilization proposed for the SE Pacific (Fig. 8g). In the absence of an immediate diatom fertilization effect from Fe or silicic acid, we hypothesize that any change in phytoplankton bloom dynamics within Reloncaví Fjord was mainly a 'top-down' effect driven by the physical interaction of ash and different ecological groups in a nutrient replete environment, rather than a 'bottom-up' effect driven by alleviation of nutrient-limitation from ash dissolution.

4.2 Volcanic ash as a unique source of trace elements

The release of the bioessential elements Fe and Mn from ash here ranged from 53 - 1200 nmol g^{-1} (dFe) and 48 - 71 nmol g^{-1} (dissolved Mn). For dFe this is comparable to the rates determined in other studies under similar experimental conditions for subduction zone volcanic ash, with reported Fe-release in prior work ranging 2-570 nmol g^{-1} (Sup. Table 1). For Mn, less prior work is available, but these values are within the 17-1300 nmol g^{-1} range reported by Hoffmann et al., (2012). Fe(II) release was particularly efficient at ash loadings <5 mg L^{-1} (Fig. 7), whereas dFe release was less sensitive to ash loading (Fig. 6). The timing of Fe(II) release in the first 60 s of incubations suggests a fast dissolution process. Fe(II) is short lived in oxic surface seawater with an observed half-life of only 10-20 minutes even in the Southern Ocean where cold surface waters slow Fe(II) oxidation (Sarthou et al., 2011). Yet, relative to Fe(III), Fe(II) is also more soluble and, from an energetic perspective, expected to be more bioaccessible to cellular uptake (Sunda et al., 2001). Whilst it is known that the vast majority of dFe leached from ash into seawater tends to occur in the first minutes of ash addition (Duggen et al., 2007; Jones and Gislason, 2008), and this could be consistent with rapid dissolution of highly soluble phases on ash surfaces, we note that there is not yet conclusive evidence concerning the precise origin of this dFe pulse. Fe(II) salts may be present on the surface of ash particles (Horwell et al., 2003; Hoshyaripour et al., 2015) and

thus the Fe(II) observed herein (Fig. 7) may reflect almost instantaneous release following dissolution of thin layers of salt coatings in ash surfaces (Ayris and Delmelle, 2012; Delmelle et al., 2007; Olsson et al., 2013). Alternatively Fe(II) could be released from more crystalline Fe(II) phases. Prior work, at much lower pH (pH 1 H_2SO_4 representing conditions that ash surfaces may experience during atmospheric processing, but not in aquatic environments) suggests that short-term release of Fe(II) or Fe(III) is determined by the surface Fe(II)/Fe ratio which may differ from the bulk Fe(II)/Fe ratio due to plume processing (Maters et al., 2017).

Different leaching protocols are widely recognised as a major challenge for interpreting and comparing different dissolution experiment datasets for all types of aerosols (Duggen et al., 2007; Morton et al., 2013). When Fe(II) is released into solution as a considerable fraction of the total dFe release this is particularly challenging to monitor, as Fe(II) oxidises on timescales of seconds to minutes depending on temperature, pH and O_2 conditions (Santana-Casiano et al., 2005). The dFe and Fe(II) leaching protocols used herein are only comparable qualitatively, as the Fe(II) method using cooler seawater and larger seawater volumes was specifically designed to test for the presence of rapid Fe(II) release and to evaluate the short-term temporal trend of any such release. Yet, for rough comparative purposes, the Fe(II) released was equivalent to 38 ± 25% (mean ± standard deviation) of dFe released at ash loadings from 1-10 mg L^{-1} and 19 ± 17% of dFe for ash loadings from 10-50 mg L^{-1}. These values are reasonably comparable to the 26% median Fe(II)/dFe fraction measured in Fe released into seawater from aerosols collected across zonal transects of the Pacific Ocean (Buck et al., 2013) suggesting that fresh Calbuco ash is roughly comparable in terms of Fe(II) lability to these environmentally processed aerosols.

4.3 A potential fertilization effect in the SE Pacific

Experiments with ash suspensions have shown that ash loading has a restricted impact on satellite chlorophyll-a retrieval (Browning et al., 2015), therefore offering a means to assess the potential biological impact of the 2015 Calbuco eruption in offshore waters. We found evidence for fertilization of offshore Pacific seawaters in the studied area (Fig. 8). Following the eruption date, mean chlorophyll-a concentrations increased ~2.5 times over a broad region where elevated UV aerosol index was detected (Fig. 8G). Both the timing and location of this chlorophyll-a peak were consistent with ash fertilization, with the peak of elevated chlorophyll-a being located within the core of highest atmospheric aerosol loading, and the peak date occurring one day after the main passage of the atmospheric aerosol plume. A similar phytoplankton response timeframe was reported following ash deposition in the NE Pacific following the August 2008 Kasatochi eruption (Hamme et al., 2010) which was similarly thought to be triggered by relief of Fe-limitation (Langmann et al., 2010). At the same time, a control region to the south of the ash-impacted Pacific region showed no clear changes in chlorophyll-a matching that observed in the higher UV aerosol index region to the north (Sup. Fig. 3).

In the SW Atlantic, two ash impacted areas are highlighted; one to the north (Fig. 8), and one to the south of the Rio de la Plata (Sup. Fig. 3). Nitrate levels are expected to be higher in the south than to the north, with Fe levels expected to be elevated across both locations as a result of their position on the continental shelf. In the area to the north of the Rio de la Plata (Fig. 8), ash deposition indicated by the UV aerosol index did not lead to such a clear corresponding change in chlorophyll-a concentrations (Fig. 8H), although with the available data it is not possible to rule out the possibility of fertilisation completely (e.g., whilst also being proceeded by a larger chlorophyll-a peak on 21 April, there is a peak in chlorophyll-a

at 25 April coinciding with elevated UV aerosol index). Phytoplankton growth in this region of the Atlantic is expected to be limited by fixed nitrogen availability, as a result of strong stratification (Moore et al., 2013) and thus dFe release from ash particles alone would not be expected to result in short-term increases to primary production. In the second area of ash deposition, to the south (Sup. Fig. 3), a chlorophyll-a peak was evident 7 days after the UV aerosol peak. However, this was not well constrained due to poor satellite coverage in the period after the eruption. Considering the dynamic spatial and temporal variation in chlorophyll within this coastal area, it is challenging to associate any change in chlorophyll specifically with ash arrival.

The change in chlorophyll-a observed in the SE Pacific contrasts with results in Reloncaví Fjord where phytoplankton abundances likely peaked much later than the first ash arrival- after 28 April. The fertilized region of the Pacific (Fig. 8) hosts upwelling of deep waters, supplying nutrients in ratios that are deficient in dFe (Bonnet et al., 2008; Torres and Ampuero, 2009). Fe-limitation of phytoplankton growth in this region is therefore anticipated, which could have been temporarily relieved following ash deposition and dFe release (Fig. 6). The differential responses observed in the Pacific and Atlantic are therefore consistent with the anticipated nutrient limitation regimes (Fe-limited and nitrogen-limited, respectively), and the supply of dFe but not fixed N (NO_3 or NH_4) from the Calbuco ash (Fig. 6 and Table 2).

5 Conclusions

The contrasting effects of volcanic ash on primary producers in Reloncaví Fjord, the SE Pacific and SW Atlantic Oceans support the hypothesis that the response of primary

728 producers is dependent on both the ash loading and the resources limiting primary production
729 in a region at a specific time of year. Leach experiments using ash from the 2015 Calbuco
730 eruption demonstrated a small increase in the alkalinity of de-ionized water from fine, but
731 not coarse ash, and no significant addition of fixed nitrogen (quantified as NO_3 and NH_4) into
732 solution. In saline waters, release of dissolved trace metals including Mn, Cu, Co, Pb, Fe and
733 specifically Fe(II) was evident.
734
735 Strong evidence of a broad-scale 'bottom-up' fertilization effect of ash on primary production
736 was not found locally within Reloncaví Fjord, although it is possible that the timing and peak
737 diatom abundance of the autumn phytoplankton bloom may have shifted in response to high
738 ash loading in the weeks following the first eruption. High diatom abundances at some
739 stations within the fjord several weeks after the eruption may have arisen from a 'top-down'
740 effect of ash on filter feeders, although the mechanism can only be speculated herein. No
741 clear positive effect of ash deposition on chlorophyll-a was evident in the SW Atlantic,
742 consistent with expected patterns in nutrient deficiency which suggest the region to be
743 nitrogen-limited. However, in offshore waters of the SE Pacific where Fe is anticipated to
744 limit phytoplankton growth, a chlorophyll-a increase was related with maximum ash
745 deposition and we presume that this increase in chlorophyll-a was likely driven by Fe-
746 fertilization.
747
748 **6. Data availability**
749 The complete 2015 time series from the Reloncaví Fjord mooring is available online
750 (https://figshare.com/articles/Puelo_Bouy/7754258). Source data for Figures 4-7 is included
751 in the Supplement.

7. Acknowledgements

The authors thank the Dirección de Investigación & Desarrollo UACh for its partial support during this project. The data presented are part of the second chapter of the PhD Thesis of MVJ at Universidad Austral de Chile. Cristian Vargas (Universidad de Concepción) is thanked for making additional chlorophyll a data available, Manuel Díaz for providing Fig. 1, Lorena Rebolledo for running the particle size test, Miriam Beck for assistance with Fe(II) flow injection analysis and 3 reviewers for constructive comments that improved the manuscript.

8. Funding

JLI and EA gratefully acknowledge funding from the European Commission (OCEAN-CERTAIN, FP7- ENV- 2013-6.1-1; no: 603773). JLI received funding by CONICYT-FONDECYT 1141065 and is partially funded by Center IDEAL (FONDAP 15150003). Partial funding came from CONICYT-FONDECYT 1140385 (RT). MVJ received financial support from a CONICYT Scholarship (Beca Doctorado Nacional 2015 No 21150285). IR and MH received funding from the Deutsche Forschungsgemeinschaft as part of Sonderforschungsbereich (SFB) 754: 'Climate-Biogeochemistry Interactions in the Tropical Ocean'.

9. Author contributions

MVJ, MH, JLI and EA designed the study. MVJ, IR, MH, RT and BR conducted analytical and field work. TB conducted satellite data analysis. MV, MH and TB wrote the initial manuscript with all authors contributing to its revision.

10. References

Achterberg, E. ., Moore, C. M., Henson, S. A., Steigenberger, S., Stohl, A., Eckhardt, S., Avendano, L. C., Cassidy, M., Hembury, D., Klar, J. K., Lucas, M. I., MacEy, A. I., Marsay, C. M. and Ryan-Keogh, T. J.: Natural iron fertilization by the Eyjafjallajokull volcanic eruption, Geophys. Res. Lett., 40(5), 921–926, doi:10.1002/grl.50221, 2013.

Ahumada, R., Rudolph, A., Gonzalez, E., Fones, G., Saldias, G. and Ahumada Rudolph, R.: Dissolved trace metals in the water column of Reloncavi Fjord, Chile, Lat. Am. J. Aquat. Res., 39, 567–574, doi:10.3856/vol39-issue3-fulltext-16, 2011.

Ayris, P. and Delmelle, P.: Volcanic and atmospheric controls on ash iron solubility: A review, Phys. Chem. Earth, doi:10.1016/j.pce.2011.04.013, 2012.

Baker, A. R. and Croot, P. L.: Atmospheric and marine controls on aerosol iron solubility in seawater, Mar. Chem., 120(1–4), 4–13, doi:10.1016/j.marchem.2008.09.003, 2010.

Balseiro, E., Souza, M. S., Olabuenaga, I. S., Wolinski, L., Navarro, M. B., Laspoumaderes, C. and Modenutti, B.: Effect of the Puyehue-Cordon Caulle volcanic complex eruption on crustacean zooplankton of Andean Lakes, Ecol. Austral, 24, 75–82, 2014.

Bonnet, S., Guieu, C., Bruyant, F., Prášil, O., Van Wambeke, F., Raimbault, P., Moutin, T., Grob, C., Gorbunov, M. Y., Zehr, J. P., Masquelier, S. M., Garczarek, L. and Claustre, H.: Nutrient limitation of primary productivity in the Southeast Pacific (BIOSOPE cruise), Biogeosciences, 5(1), 215–225, doi:10.5194/bg-5-215-2008, 2008.

Boyle, E. A., Edmond, J. M. and Sholkovitz, E. R.: Mechanism of iron removal in estuaries, Geochim. Cosmochim. Acta, 41(9), 1313–1324, doi:10.1016/0016-7037(77)90075-8, 1977.

800 Browning, T. J., Bouman, H. A., Henderson, G. M., Mather, T. A., Pyle, D. M., Schlosser,
801 C., Woodward, E. M. S. and Moore, C. M.: Strong responses of Southern Ocean
802 phytoplankton communities to volcanic ash, Geophys. Res. Lett., 41(8), 2851–2857,
803 doi:10.1002/2014GL059364, 2014.
804 Browning, T. J., Stone, K., Bouman, H., Mather, T. A., Pyle, D. M., Moore, M. and
805 Martinez-Vicente, V.: Volcanic ash supply to the surface ocean – remote sensing of
806 biological responses and their wider biogeochemical significance, Front. Mar. Sci., 2,
807 doi:10.3389/fmars.2015.00014, 2015.
808 Brzezinski, M. A.: The Si:C:N ratio of marine diatoms: interspecific variability and the
809 effect of some environmental variables, J. Phycol., 21(3), 347–357, doi:10.1111/j.0022-
810 3646.1985.00347.x, 1985.
811 Buck, C. S., Landing, W. M. and Resing, J.: Pacific Ocean aerosols: Deposition and
812 solubility of iron, aluminum, and other trace elements, Mar. Chem., 157, 117–130,
813 doi:10.1016/j.marchem.2013.09.005, 2013.
814 Cáceres, M., Valle-Levinson, A., Sepúlveda, H. H. and Holderied, K.: Transverse
815 variability of flow and density in a Chilean fjord, in Continental Shelf Research., 2002.
816 Castillo, M. I., Cifuentes, U., Pizarro, O., Djurfeldt, L. and Caceres, M.: Seasonal
817 hydrography and surface outflow in a fjord with a deep sill: The Reloncaví fjord, Chile,
818 Ocean Sci., 12, 533–544, doi:10.5194/os-12-533-2016, 2016.
819 DeGrandpre, M. D., Hammar, T. R., Smith, S. P. and Sayles, F. L.: In situ measurements of
820 seawater pCO2, Limnol. Oceanogr., 40(5), 969–975, doi:10.4319/lo.1995.40.5.0969, 1995.
821 DeGrandpre, M. D., Baehr, M. M. and Hammar, T. R.: Calibration-free optical chemical
822 sensors, Anal. Chem., 71(6), 1152–1159, doi:10.1021/ac9805955, 1999.
823 Delmelle, P., Lambert, M., Dufrêne, Y., Gerin, P. and Óskarsson, N.: Gas/aerosol-ash

824 interaction in volcanic plumes: New insights from surface analyses of fine ash particles,
825 Earth Planet. Sci. Lett., 259, 159–170, doi:10.1016/j.epsl.2007.04.052, 2007.
826 Duggen, S., Croot, P., Schacht, U. and Hoffmann, L.: Subduction zone volcanic ash can
827 fertilize the surface ocean and stimulate phytoplankton growth: Evidence from
828 biogeochemical experiments and satellite data, Geophys. Res. Lett.,
829 doi:10.1029/2006GL027522, 2007.
830 Duggen, S., Olgun, N., Croot, P., Hoffmann, L., Dietze, H., Delmelle, P. and Teschner, C.:
831 The role of airborne volcanic ash for the surface ocean biogeochemical iron-cycle: a
832 review, Biogeosciences, 7(3), 827–844, doi:10.5194/bg-7-827-2010, 2010.
833 Van Eaton, A. R., Amigo, Á., Bertin, D., Mastin, L. G., Giacosa, R. E., González, J.,
834 Valderrama, O., Fontijn, K. and Behnke, S. A.: Volcanic lightning and plume behavior
835 reveal evolving hazards during the April 2015 eruption of Calbuco volcano, Chile,
836 Geophys. Res. Lett., 43(7), 3563–3571, doi:10.1002/2016GL068076, 2016.
837 Ermolin, M. S., Fedotov, P. S., Malik, N. A. and Karandashev, V. K.: Nanoparticles of
838 volcanic ash as a carrier for toxic elements on the global scale, Chemosphere, 200, 16–22,
839 doi:10.1016/j.chemosphere.2018.02.089, 2018.
840 Frogner, P., Gislason, S. R. and Oskarsson, N.: Fertilizing potential of volcanic ash in
841 ocean surface water, Geology, 29(6), 487–490, doi:10.1130/0091-
842 7613(2001)029<0487:fpovai>2.0.co;2, 2001.
843 Gledhill, M. and Buck, K. N.: The organic complexation of iron in the marine environment:
844 a review, Front. Microbiol., 3, 69, doi:10.3389/fmicb.2012.00069, 2012.
845 González, H. E., Calderón, M. J., Castro, L., Clement, A., Cuevas, L. A., Daneri, G., Iriarte,
846 J. L., Lizárraga, L., Martínez, R., Menschel, E., Silva, N., Carrasco, C., Valenzuela, C.,
847 Vargas, C. A. and Molinet, C.: Primary production and plankton dynamics in the Reloncaví

Fjord and the Interior Sea of Chiloé, Northern Patagonia, Chile, Mar. Ecol. Prog. Ser., 402, 13–30, 2010.

Hamme, R. C., Webley, P. W., Crawford, W. R., Whitney, F. A., Degrandpre, M. D., Emerson, S. R., Eriksen, C. C., Giesbrecht, K. E., Gower, J. F. R., Kavanaugh, M. T., Pea, M. A., Sabine, C. L., Batten, S. D., Coogan, L. A., Grundle, D. S. and Lockwood, D.: Volcanic ash fuels anomalous plankton bloom in subarctic northeast Pacific, Geophys. Res. Lett., 37(19), L19604, doi:10.1029/2010GL044629, 2010.

Haraldsson, C., Anderson, L. G., Hassellöv, M., Hulth, S. and Olsson, K.: Rapid, high-precision potentiometric titration of alkalinity in ocean and sediment pore waters, Deep Sea Res. Part I Oceanogr. Res. Pap., 44(12), 2031–2044, doi:10.1016/S0967-0637(97)00088-5, 1997.

Hoffmann, L. J., Breitbarth, E., Ardelan, M. V., Duggen, S., Olgun, N., Hassellöv, M. and Wängberg, S.-Å.: Influence of trace metal release from volcanic ash on growth of Thalassiosira pseudonana and Emiliania huxleyi, Mar. Chem., 132–133, 28–33, doi:10.1016/j.marchem.2012.02.003, 2012.

Hopwood, M. J., Santana-González, C., Gallego-Urrea, J., Sanchez, N., Achterberg, E. P., Ardelan, M. V., Gledhill, M., González-Dávila, M., Hoffmann, L., Leiknes, Ø., Magdalena Santana-Casiano, J., Tsagaraki, T. M. and Turner, D.: Fe(II) stability in coastal seawater during experiments in Patagonia, Svalbard, and Gran Canaria, Biogeosciences, doi:10.5194/bg-17-1327-2020, 2020.

Horwell, C. J., Fenoglio, I., Vala Ragnarsdottir, K., Sparks, R. S. J. and Fubini, B.: Surface reactivity of volcanic ash from the eruption of Soufrière Hills volcano, Montserrat, West Indies with implications for health hazards, Environ. Res., 93(2), 202–215, doi:10.1016/S0013-9351(03)00044-6, 2003.

872 Hoshyaripour, G. A., Hort, M. and Langmann, B.: Ash iron mobilization through
873 physicochemical processing in volcanic eruption plumes: A numerical modeling approach,
874 Atmos. Chem. Phys., 15, 9361–9379, doi:10.5194/acp-15-9361-2015, 2015.
875 Hu, C., Lee, Z. and Franz, B.: Chlorophyll aalgorithms for oligotrophic oceans: A novel
876 approach based on three-band reflectance difference, J. Geophys. Res. Ocean., 117(C1),
877 doi:10.1029/2011JC007395, 2012.
878 Iriarte, J. L., González, H. E., Liu, K. K., Rivas, C. and Valenzuela, C.: Spatial and
879 temporal variability of chlorophyll and primary productivity in surface waters of southern
880 Chile (41.5–43° S), Estuar. Coast. Shelf Sci., 74(3), 471–480,
881 doi:10.1016/j.ecss.2007.05.015, 2007.
882 Jones, M. R., Nightingale, P. D., Turner, S. M. and Liss, P. S.: Adaptation of a load-inject
883 valve for a flow injection chemiluminescence system enabling dual-reagent injection
884 enhances understanding of environmental Fenton chemistry, Anal. Chim. Acta, 796, 55–60,
885 doi:10.1016/j.aca.2013.08.003, 2013.
886 Jones, M. T. and Gislason, S. R.: Rapid releases of metal salts and nutrients following the
887 deposition of volcanic ash into aqueous environments, Geochim. Cosmochim. Acta, 72(15),
888 3661–3680, doi:10.1016/j.gca.2008.05.030, 2008.
889 Labbé-Ibáñez, P., Iriarte, J. L. and Pantoja, S.: Respuesta del microfitoplancton a la adición
890 de nitrato y ácido silícico en fiordos de la Patagonia chilena, Lat. Am. J. Aquat. Res., 43(1),
891 80–93, doi:10.3856/vol43-issue1-fulltext-8, 2015.
892 Langmann, B., Zakšek, K., Hort, M. and Duggen, S.: Volcanic ash as fertiliser for the
893 surface ocean, Atmos. Chem. Phys., 10, 3891–3899, doi:10.5194/acp-10-3891-2010, 2010.
894 León-Muñoz, J., Marcé, R. and Iriarte, J. L.: Influence of hydrological regime of an Andean
895 river on salinity, temperature and oxygen in a Patagonia fjord, Chile, New Zeal. J. Mar.

Freshw. Res., 47(4), 515–528, doi:10.1080/00288330.2013.802700, 2013.

León-Muñoz, J., Urbina, M. A., Garreaud, R. and Iriarte, J. L.: Hydroclimatic conditions trigger record harmful algal bloom in western Patagonia (summer 2016), Sci. Rep., 8(1), 1330, doi:10.1038/s41598-018-19461-4, 2018.

Lin, I. I., Hu, C., Li, Y. H., Ho, T. Y., Fischer, T. P., Wong, G. T. F., Wu, J., Huang, C. W., Chu, D. A., Ko, D. S. and Chen, J. P.: Fertilization potential of volcanic dust in the low-nutrient low-chlorophyll western North Pacific subtropical gyre: Satellite evidence and laboratory study, Global Biogeochem. Cycles, 25, GB1006, doi:10.1029/2009GB003758, 2011.

López-Escobar, L., Parada, M. A., Hickey-Vargas, R., Frey, F. A., Kempton, P. D. and Moreno, H.: Calbuco Volcano and minor eruptive centers distributed along the Liquiñe-Ofqui Fault Zone, Chile (41°–42° S): contrasting origin of andesitic and basaltic magma in the Southern Volcanic Zone of the Andes, Contrib. to Mineral. Petrol., 119(4), 345–361, doi:10.1007/BF00286934, 1995.

Martin, J. H., Fitzwater, S. E. and Gordon, R. M.: Iron deficiency limits phytoplankton growth in Antarctic waters, Global Biogeochem. Cycles, 4(1), 5–12, 1990.

Maters, E. C., Delmelle, P. and Gunnlaugsson, H. P.: Controls on iron mobilisation from volcanic ash at low pH: Insights from dissolution experiments and Mössbauer spectroscopy, Chem. Geol., 449, 73–81, doi:10.1016/j.chemgeo.2016.11.036, 2017.

Mélançon, J., Levasseur, M., Lizotte, M., Delmelle, P., Cullen, J., Hamme, R. C., Peña, A., Simpson, K. G., Scarratt, M., Tremblay, J. É., Zhou, J., Johnson, K., Sutherland, N., Arychuk, M., Nemcek, N. and Robert, M.: Early response of the northeast subarctic Pacific plankton assemblage to volcanic ash fertilization, Limnol. Oceanogr., 59, doi:10.4319/lo.2014.59.1.0055, 2014.

Mendez, J., Guieu, C. and Adkins, J.: Atmospheric input of manganese and iron to the ocean: Seawater dissolution experiments with Saharan and North American dusts, Mar. Chem., 120(1), 34–43, doi:10.1016/j.marchem.2008.08.006, 2010.

Millero, F. J., Sotolongo, S. and Izaguirre, M.: The oxidation-kinetics of Fe(II) in seawater, Geochim. Cosmochim. Acta, 51(4), 793–801, doi:10.1016/0016-7037(87)90093-7, 1987.

Molinet, C., Díaz, M., Marín, S. L., Astorga, M. P., Ojeda, M., Cares, L. and Asencio, E.: Relation of mussel spatfall on natural and artificial substrates: Analysis of ecological implications ensuring long-term success and sustainability for mussel farming, Aquaculture, 467, 211–218, doi:10.1016/j.aquaculture.2016.09.019, 2017.

Moore, C. M., Mills, M. M., Arrigo, K. R., Berman-Frank, I., Bopp, L., Boyd, P. W., Galbraith, E. D., Geider, R. J., Guieu, C., Jaccard, S. L., Jickells, T. D., La Roche, J., Lenton, T. M., Mahowald, N. M., Marañón, E., Marinov, I., Moore, J. K., Nakatsuka, T., Oschlies, A., Saito, M. A., Thingstad, T. F., Tsuda, A. and Ulloa, O.: Processes and patterns of oceanic nutrient limitation, Nat. Geosci., doi:10.1038/ngeo1765, 2013.

Morton, P. L., Landing, W. M., Hsu, S. C., Milne, A., Aguilar-Islas, A. M., Baker, A. R., Bowie, A. R., Buck, C. S., Gao, Y., Gichuki, S., Hastings, M. G., Hatta, M., Johansen, A. M., Losno, R., Mead, C., Patey, M. D., Swarr, G., Vandermark, A. and Zamora, L. M.: Methods for the sampling and analysis of marine aerosols: Results from the 2008 GEOTRACES aerosol intercalibration experiment, Limnol. Oceanogr. Methods, 11, doi:10.4319/lom.2013.11.62, 2013.

Mosley, L. M., Husheer, S. L. G. and Hunter, K. A.: Spectrophotometric pH measurement in estuaries using thymol blue and m-cresol purple, Mar. Chem., 91, 175–186, doi:10.1016/j.marchem.2004.06.008, 2004.

Newcomb, T. W. and Flagg, T. A.: Some effects of Mt. St. Helens volcanic ash on juvenile

944 salmon smolts., Mar. Fish. Rev., 45(2), 8–12, 1983.
945 Olgun, N., Duggen, S., Croot, P. L., Delmelle, P., Dietze, H., Schacht, U., Óskarsson, N.,
946 Siebe, C., Auer, A. and Garbe-Schönberg, D.: Surface ocean iron fertilization: The role of
947 airborne volcanic ash from subduction zone and hot spot volcanoes and related iron fluxes
948 into the Pacific Ocean, Global Biogeochem. Cycles, 25(4), doi:10.1029/2009GB003761,
949 2011.
950 Olsson, J., Stipp, S. L. S., Dalby, K. N. and Gislason, S. R.: Rapid release of metal salts and
951 nutrients from the 2011 Grímsvötn, Iceland volcanic ash, Geochim. Cosmochim. Acta,
952 doi:10.1016/j.gca.2013.09.009, 2013.
953 Óskarsson, N.: The interaction between volcanic gases and tephra: Fluorine adhering to
954 tephra of the 1970 hekla eruption, J. Volcanol. Geotherm. Res., doi:10.1016/0377-
955 0273(80)90107-9, 1980.
956 Rapp, I., Schlosser, C., Rusiecka, D., Gledhill, M. and Achterberg, E. P.: Automated
957 preconcentration of Fe, Zn, Cu, Ni, Cd, Pb, Co, and Mn in seawater with analysis using
958 high-resolution sector field inductively-coupled plasma mass spectrometry, Anal. Chim.
959 Acta, 976, 1–13, doi:10.1016/j.aca.2017.05.008, 2017.
960 Reckziegel, F., Bustos, E., Mingari, L., Báez, W., Villarosa, G., Folch, A., Collini, E.,
961 Viramonte, J., Romero, J. and Osores, S.: Forecasting volcanic ash dispersal and coeval
962 resuspension during the April-May 2015 Calbuco eruption, J. Volcanol. Geotherm. Res.,
963 doi:10.1016/j.jvolgeores.2016.04.033, 2016.
964 Rogan, N., Achterberg, E. P., Le Moigne, F. A. C., Marsay, C. M., Tagliabue, A. and
965 Williams, R. G.: Volcanic ash as an oceanic iron source and sink, Geophys. Res. Lett.,
966 43(6), 2732–2740, doi:10.1002/2016GL067905, 2016.
967 Romero, J. E., Morgavi, D., Arzilli, F., Daga, R., Caselli, A., Reckziegel, F., Viramonte, J.,

968 Díaz-Alvarado, J., Polacci, M., Burton, M. and Perugini, D.: Eruption dynamics of the 22–
969 23 April 2015 Calbuco Volcano (Southern Chile): Analyses of tephra fall deposits, J.
970 Volcanol. Geotherm. Res., 317, 15–29, doi:10.1016/j.jvolgeores.2016.02.027, 2016.
971 Rubin, C. H., Noji, E. K., Seligman, P. J., Holtz, J. L., Grande, J. and Vittani, F.:
972 Evaluating a fluorosis hazard after a volcanic eruption, Arch. Environ. Health,
973 doi:10.1080/00039896.1994.9954992, 1994.
974 Sanchez, N., Bizsel, N., Iriarte, J. L., Olsen, L. M. and Ardelan, M. V.: Iron cycling in a
975 mesocosm experiment in a north Patagonian fjord: Potential effect of ammonium addition
976 by salmon aquaculture, Estuar. Coast. Shelf Sci., 220, 209–219,
977 doi:10.1016/j.ecss.2019.02.044, 2019.
978 Santana-Casiano, J. M., Gonzaalez-Davila, M. and Millero, F. J.: Oxidation of nanomolar
979 levels of Fe(II) with oxygen in natural waters, Environ. Sci. Technol., 39(7), 2073–2079,
980 doi:10.1021/es049748y, 2005.
981 Sarmiento, J. L.: Atmospheric CO2 stalled, Nature, doi:10.1038/365697a0, 1993.
982 Sarthou, G., Bucciarelli, E., Chever, F., Hansard, S. P., Gonzalez-Davila, M., Santana-
983 Casiano, J. M., Planchon, F. and Speich, S.: Labile Fe(II) concentrations in the Atlantic
984 sector of the Southern Ocean along a transect from the subtropical domain to the Weddell
985 Sea Gyre, Biogeosciences, 8(9), 2461–2479, doi:10.5194/bg-8-2461-2011, 2011.
986 Seidel, M. P., DeGrandpre, M. D. and Dickson, A. G.: A sensor for in situ indicator-based
987 measurements of seawater pH, Mar. Chem., 109(1), 18–28,
988 doi:10.1016/j.marchem.2007.11.013, 2008.
989 Simonella, L. E., Palomeque, M. E., Croot, P. L., Stein, A., Kupczewski, M., Rosales, A.,
990 Montes, M. L., Colombo, F., García, M. G., Villarosa, G. and Gaiero, D. M.: Soluble iron
991 inputs to the Southern Ocean through recent andesitic to rhyolitic volcanic ash eruptions

992 from the Patagonian Andes, Global Biogeochem. Cycles, 29(8), 1125–1144,
993 doi:10.1002/2015GB005177, 2015.
994 Siringan, F. P., Racasa, E. D. R., David, C. P. C. and Saban, R. C.: Increase in Dissolved
995 Silica of Rivers Due to a Volcanic Eruption in an Estuarine Bay (Sorsogon Bay,
996 Philippines), Estuaries and Coasts, 41, 2277–2288, doi:10.1007/s12237-018-0428-1, 2018.
997 Stewart, C., Johnston, D. M., Leonard, G. S., Horwell, C. J., Thordarson, T. and Cronin, S.
998 J.: Contamination of water supplies by volcanic ashfall: A literature review and simple
999 impact modelling, J. Volcanol. Geotherm. Res., 158(3), 296–306,
1000 doi:10.1016/j.jvolgeores.2006.07.002, 2006.
1001 Sunda, W. G., Buffle, J. and Van Leeuwen, H. P.: Bioavailability and Bioaccumulation of
1002 Iron in the Sea, in The Biogeochemistry of Iron in Seawater, vol. 7, edited by D. R. Turner
1003 and K. A. Hunter, pp. 41–84, John Wiley & Sons, Ltd, Chichester., 2001.
1004 Torres, O., Tanskanen, A., Veihelmann, B., Ahn, C., Braak, R., Bhartia, P. K., Veefkind, P.
1005 and Levelt, P.: Aerosols and surface UV products form Ozone Monitoring Instrument
1006 observations: An overview, J. Geophys. Res. Atmos., doi:10.1029/2007JD008809, 2007.
1007 Torres, R. and Ampuero, P.: Strong CO2 outgassing from high nutrient low chlorophyll
1008 coastal waters off central Chile (30°S): The role of dissolved iron, Estuar. Coast. Shelf Sci.,
1009 83(2), 126–132, doi:10.1016/j.ecss.2009.02.030, 2009.
1010 Torres, R., Silva, N., Reid, B. and Frangopulos, M.: Silicic acid enrichment of subantarctic
1011 surface water from continental inputs along the Patagonian archipelago interior sea (41-
1012 56°S), Prog. Oceanogr., 129, 50–61, doi:10.1016/j.pocean.2014.09.008, 2014.
1013 Utermöhl, H.: Zur Vervollkommnung der quantitativen Phytoplankton-Methodik, SIL
1014 Commun. 1953-1996, doi:10.1080/05384680.1958.11904091, 1958.
1015 Vergara-Jara, M. J., DeGrandpre, M. D., Torres, R., Beatty, C. M., Cuevas, L. A., Alarcón,

E. and Iriarte, J. L.: Seasonal Changes in Carbonate Saturation State and Air-Sea CO2 Fluxes During an Annual Cycle in a Stratified-Temperate Fjord (Reloncaví Fjord, Chilean Patagonia), J. Geophys. Res. Biogeosciences, 124(9), 2851–2865, doi:10.1029/2019JG005028, 2019.

Watson, A. J.: Volcanic iron, CO2, ocean productivity and climate, Nature, doi:10.1038/385587b0, 1997.

Weinbauer, M. G., Guinot, B., Migon, C., Malfatti, F. and Mari, X.: Skyfall - neglected roles of volcano ash and black carbon rich aerosols for microbial plankton in the ocean, J. Plankton Res., 39(2), 187–198, doi:10.1093/plankt/fbw100, 2017.

Welschmeyer, N. A.: Fluorometric analysis of chlorophyll a in the presence of chlorophyll b and pheopigments, Limnol. Oceanogr., doi:10.4319/lo.1994.39.8.1985, 1994.

Witham, C. S., Oppenheimer, C. and Horwell, C. J.: Volcanic ash-leachates: a review and recommendations for sampling methods, J. Volcanol. Geotherm. Res., 141(3), 299–326, doi:10.1016/j.jvolgeores.2004.11.010, 2005.

Wolinski, L., Laspoumaderes, C., Bastidas Navarro, M., Modenutti, B. and Balseiro, E.: The susceptibility of cladocerans in North Andean Patagonian lakes to volcanic ashes, Freshw. Biol., 58, 1878–1888, doi:10.1111/fwb.12176, 2013.

Yevenes, M. A., Lagos, N. A., Farías, L. and Vargas, C. A.: Greenhouse gases, nutrients and the carbonate system in the Reloncaví Fjord (Northern Chilean Patagonia): Implications on aquaculture of the mussel, Mytilus chilensis, during an episodic volcanic eruption, Sci. Total Environ., doi:10.1016/j.scitotenv.2019.03.037, 2019.